

**MICROIONTOPHORESIS AS A TECHNIQUE TO INVESTIGATE SPIKE TIMING  
DEPENDENT PLASTICITY**

by

**Joyeeta Dutta-Moscato**

BSE, BA, University of Pennsylvania, 2000

Submitted to the Graduate Faculty of  
Arts & Sciences in partial fulfillment  
of the requirements for the degree of  
Master of Science

University of Pittsburgh

2007

UNIVERSITY OF PITTSBURGH  
FACULTY OF ARTS & SCIENCES

This thesis was presented

by

Joyeeta Dutta-Moscato

It was defended on

November 15, 2007

and approved by

Karl Kandler, PhD, Center for Neuroscience

Alison Barth, PhD, Center for Neuroscience

Guoqiang Bi, PhD, Center for Neuroscience

Thesis Advisor: Jon W. Johnson, PhD, Center for Neuroscience

Copyright © by Joyeeta Dutta-Moscato

2007

**MICROIONTOPHORESIS AS A TECHNIQUE TO INVESTIGATE SPIKE TIMING  
DEPENDENT PLASTICITY**

Joyeeta Dutta-Moscato, M.S.

University of Pittsburgh, December 2007

Spike timing dependent plasticity (STDP) is a form of synaptic plasticity that depends on the relative time of activation of a presynaptic neuron and its postsynaptic neuron. STDP in the synapses made by Schaffer collateral afferents onto hippocampal CA1 pyramidal neurons (CA3-CA1 synapses) is NMDA receptor dependent. The objective of the current study was to develop and test a technique of glutamate iontophoresis that could replace the role of presynaptic neurotransmitter release at the CA3-CA1 synapse, so that the postsynaptic mechanisms involved in the induction of STDP could be isolated for study. Therefore, this document describes: (1) fabrication of electrodes that could be used for millisecond-level microiontophoresis in acute slice preparations of the juvenile rat hippocampus; (2) characterization of the properties and limitations of microiontophoresis in slice tissue, specifically for activation of postsynaptic ionotropic glutamate receptors at the CA3-CA1 synapse; (3) induction of STDP by pairing microiontophoresis with postsynaptic depolarization; (4) characterization of the properties and limitations of microiontophoretically induced STDP. It was determined that microiontophoresis is a viable technique to study the postsynaptic mechanisms of STDP at the CA3-CA1 synapse. My results also show that microiontophoretically induced STDP exhibits many of the same general properties as STDP induced either synaptically or by exogenously applied agonists. Microiontophoretically induced STDP also exhibits other features that will need to be considered during the design and interpretation of further experiments.

## TABLE OF CONTENTS

<b>ACKNOWLEDGEMENTS .....</b>	<b>IX</b>
<b>1.0 INTRODUCTION.....</b>	<b>1</b>
<b>1.1 NMDA RECEPTOR DEPENDENT LONG TERM POTENTIATION AND DEPRESSION AT THE CA3-CA1 SYNAPSE .....</b>	<b>1</b>
<b>1.2 SPIKE TIMING DEPENDENT PLASTICITY.....</b>	<b>5</b>
<b>1.3 INVESTIGATION OF HEBBIAN PROPERTIES USING EXOGENOUS APPLICATIONS OF GLUTAMATE .....</b>	<b>7</b>
<b>2.0 MICROIONTOPHORESIS OF GLUTAMATE ON CA3-CA1 SYNAPSES.....</b>	<b>10</b>
<b>2.1 MATERIALS AND METHODS.....</b>	<b>11</b>
<b>2.1.1 Microelectrodes for iontophoresis.....</b>	<b>11</b>
<b>2.1.2 Slice preparation and Electrophysiology.....</b>	<b>16</b>
<b>3.0 RESULTS .....</b>	<b>20</b>
<b>3.1 CHARACTERIZATION OF CA1 PYRAMIDAL CELL RESPONSES TO GLUTAMATE IONTOPHORESIS .....</b>	<b>20</b>
<b>3.2 EXPLORATION OF A PARAMETER SPACE FOR IONTOPHORETICALLY INDUCED STDP .....</b>	<b>26</b>
<b>4.0 DISCUSSION .....</b>	<b>33</b>
<b>4.1 SPATIAL AND ANATOMICAL ASPECTS .....</b>	<b>33</b>

<b>4.2</b>	<b>FACTORS AFFECTING INDUCTION OF LTP VERSUS LTD .....</b>	<b>35</b>
<b>4.3</b>	<b>TECHNICAL OBSERVATIONS .....</b>	<b>38</b>
<b>5.0</b>	<b>TABLES.....</b>	<b>41</b>
<b>6.0</b>	<b>FIGURES.....</b>	<b>42</b>
	<b>BIBLIOGRAPHY.....</b>	<b>62</b>

## LIST OF TABLES

<b>Table 1.</b> Kinetics of $I_{\text{AMPA}}$ and $I_{\text{NMDA}}$	... 41
<b>Table 2.</b> $I_{\text{AMPA}}$ for different amplitudes of iontophoretic current	... 41

## LIST OF FIGURES

<b>Figure 1:</b> Characterization of the current evoked by glutamate microiontophoresis	... 42
<b>Figure 2:</b> Fidelity of iontophoretic stimulus	... 44
<b>Figure 3:</b> Reliability of glutamate evoked current over time	... 45
<b>Figure 4:</b> Glutamate iontophoresis activates fast sodium currents despite voltage clamp	... 47
<b>Figure 5:</b> Positive pairing induction protocol can lead to potentiation of glutamate evoked response (n = 5 out of 9)	... 49
<b>Figure 6:</b> Positive pairing induction protocol can lead to depression of glutamate evoked response (n = 4 out of 9)	... 51
<b>Figure 7:</b> Negative pairing induction protocol leads to depression of glutamate evoked response (n = 4 out of 4)	... 53
<b>Figure 8:</b> Induction protocol is an important determinant of STDP outcome	... 55
<b>Figure 9:</b> Initial conditions influence induction of LTP in response to positive pairing of glutamate iontophoresis and depolarization	... 56
<b>Figure 10:</b> When initial currents are < 90 pA in amplitude, positive D-I pairing results in LTP, while negative D-I pairing results in LTD	... 58
<b>Figure 11:</b> Initial conditions influence induction of LTP in response to positive pairing of glutamate iontophoresis and depolarization	... 60

## **ACKNOWLEDGEMENTS**

I would like to thank the members of my committee, Dr. Karl Kandler, Dr. Alison Barth, Dr. Guoqiang Bi and my advisor, Dr. Jon Johnson.

I would also like to thank the Center for Neuroscience faculty, staff and students.

## **1.0 INTRODUCTION**

A wide array of neurons in the mammalian central nervous system exhibit an ability to increase or decrease their influence on other neurons. This plasticity of synapses, especially in response to patterns of activity, offers a biological means of pattern recognition. Synaptic plasticity is, therefore, believed to subserve cognitive functions such as learning and memory. Evidence for a long-lasting, activity-dependent change in synaptic efficacy first appeared in the early 1970s, when it was shown that repetitive activation of excitatory synapses in the hippocampus, a brain region known to be essential for learning and memory, caused an increase in synaptic strength that could last for hours or even days<sup>11, 49</sup>. This phenomenon, known as long term potentiation (LTP), was widely studied over the following decades. A conceptually opposite phenomenon, long term depression (LTD) was also soon characterized<sup>22, 62</sup>.

### **1.1 NMDA RECEPTOR DEPENDENT LONG TERM POTENTIATION AND DEPRESSION AT THE CA3-CA1 SYNAPSE**

A model of particular interest has been the synapse made by Schaffer collateral fibers, comprised of axons of CA3 pyramidal neurons, which are afferent upon CA1 pyramidal neurons<sup>29</sup>. This is henceforth referred to as the CA3-CA1 synapse. This document focuses exclusively on plasticity

induced on a timescale of less than an hour, which may be an early form of longer lasting plasticity.

In the CA3-CA1 synapse, stimulation of the presynaptic axons causes release of glutamate onto dendrites of CA1 neurons. The released glutamate is detected by postsynaptic receptors. One type of glutamate receptor is the  $\alpha$ -amino-3-hydroxy-5-methyl-4-isoxazolepropionic (AMPA) receptor. Binding of glutamate at the AMPA receptors leads to opening of a channel permeable to monovalent cations ( $\text{Na}^+$  and  $\text{K}^+$ ), causing an inward (depolarizing) current at negative membrane potential. Another type of glutamate receptor present on dendrites of the CA1 neurons is the N-methyl-D-aspartate (NMDA) receptor. While NMDA receptors are activated by glutamate binding, they also require a coagonist, glycine, and are modulated by a voltage dependent block by  $\text{Mg}^{++}$ .<sup>35, 57</sup> The natural milieu of the brain, cerebrospinal fluid (CSF), contains magnesium, as does artificial CSF (ACSF), which is generally used in vitro; under these conditions, depolarization of the membrane from its resting membrane potential decreases blockage by  $\text{Mg}^{++}$ , increasing the inward current generated by influx of  $\text{Na}^+$  and  $\text{Ca}^{++}$ . Activation of the AMPA receptor is believed to play a role in depolarizing the membrane to enhance NMDA receptor activation. While there are some AMPA receptors which are  $\text{Ca}^{++}$  permeable themselves, such receptors are rarely found in the CA3-CA1 synapse, and are substantially less permeable to  $\text{Ca}^{++}$  than NMDA receptors.

While inhibition of the NMDA receptor does not significantly reduce the excitatory postsynaptic current evoked by regular synaptic transmission, it does affect the induction of synaptic plasticity. Influx through the NMDA receptor is an important source of rise in  $\text{Ca}^{++}$  concentration in the postsynaptic region. Opening of voltage gated calcium channels and  $\text{Ca}^{++}$ -induced  $\text{Ca}^{++}$  release also lead to rise in local  $\text{Ca}^{++}$  concentration<sup>75</sup>, but blocking  $\text{Ca}^{++}$  influx

through NMDA receptors blocks the induction of LTP and LTD<sup>66</sup>. Preventing an increase in postsynaptic  $\text{Ca}^{++}$  with  $\text{Ca}^{++}$  chelators blocks LTP, whereas directly raising the amount of postsynaptic  $\text{Ca}^{++}$  by photolysis of caged  $\text{Ca}^{++}$  can mimic LTP<sup>96</sup>. Although the precise mechanism of LTP and LTD induction is still a topic of ongoing research, it is widely accepted that both processes, at the CA3-CA1 synapse, are NMDA receptor dependent<sup>8</sup>.

Numerous  $\text{Ca}^{++}$  sensitive enzymes have been implicated in the initiation of signaling cascades that lead to LTP and LTD. Calmodulin (CaM), for example, is a protein that modulates the activity of, and confers  $\text{Ca}^{++}$  sensitivity on, several key signaling molecules that are crucial for synaptic plasticity<sup>95</sup>. Protein kinases such as  $\text{Ca}^{++}$ /CaM-dependent protein kinase II (CaMKII), bind to CaM with a higher affinity in the presence of local  $\text{Ca}^{++}$ , and CaMKII activation is known to be essential for induction of LTP in mature CA1 pyramidal neurons<sup>45, 49, 95, 97</sup>. LTP induction protocols increase  $\text{Ca}^{++}$  entry through the NMDA receptor, which increases the local concentration of  $\text{Ca}^{++}$  in the postsynaptic area, and activates CaMKII. Activation of CaMKII can increase delivery of AMPA receptors to the synaptic surface<sup>32</sup>, increase single channel conductance of AMPA receptors<sup>72</sup>, and change subunit composition of AMPA receptors<sup>71</sup>. CaMKII is one of many signaling proteins that have been implicated in the induction of NMDA receptor dependent LTP<sup>46</sup>.

LTD at the CA3-CA1 synapse is also NMDA receptor dependent, and loading the postsynaptic neuron with  $\text{Ca}^{++}$  buffers blocks LTD<sup>62</sup>. A prominent hypothesis for the induction of NMDA receptor dependent LTD proposes that a modest rise in postsynaptic calcium preferentially activates a protein phosphatase cascade, which leads to endocytosis of AMPA receptors<sup>6, 60, 61, 68</sup>. As in the case of LTP, many different classes of molecules and complex signaling cascades are believed to be involved in the induction of LTD.

There has been experimental evidence implicating the activation of NR2A-subunit containing NMDA receptors as a requirement for LTP, and the activation of NR2B-subunit containing receptors as a requirement for LTD<sup>44, 54</sup>. Since the subunit composition of NMDA receptors changes with age, the idea that subunit composition may determine the direction of plasticity gains further credence from prior observations that tetanic stimulation of CA3 afferents to CA1 pyramidal neurons are able to induce LTD more easily than LTP in neonatal animals<sup>10, 43</sup>. NR2B subunits are expressed in high levels in neonatal rats, and are seen to decrease with age, corresponding to an increase in NR2A subunit expression. High levels of NR2B proteins are found in the synapses of young rats, aged 2 days (P2) and 10 days (P10), but in adult rats NR2B levels are much lower. NR2A proteins are found in very low levels at P2, with a small increase at P10, and a large increase in adults<sup>69, 76</sup>. Accompanying this transition in subunit expression, is a greater functional presence of NR2A in synaptic receptors<sup>91</sup>. NMDA receptors containing NR2A subunits have faster kinetics than receptors containing NR2B subunits. The kinetics of NMDA excitatory postsynaptic currents (EPSC) become faster during development, and correlate with an increase in expression of the NR2A subunit and a decrease in the sensitivity to NR2B selective antagonists<sup>25, 74, 82</sup>. While the EPSCs are relatively insensitive to NR2B selective antagonists, however, extrasynaptic receptors still show considerable block by these agents<sup>58, 74, 87, 91</sup>.

It is not unequivocally clear that LTP and LTD are induced by selective activation of either NR2A or NR2B subunit containing receptors<sup>27</sup>. There have been reports of NR2A independent LTP<sup>7, 86, 90, 94</sup>. There is also evidence of CaMKII localization to NR2B containing receptors, which suggests a role for NR2B subunit containing NMDA receptors in the induction of LTP<sup>4, 5</sup>. Other factors, such as association of the NMDA receptor with different proteins, and

interactions with other voltage sensitive and metabotropic receptors, may also play a role in determining plasticity outcomes.

## 1.2 SPIKE TIMING DEPENDENT PLASTICITY

Spike timing dependent plasticity (STDP) is a form of synaptic plasticity in which the order of activation of two connected neurons leads to LTP or LTD. STDP manifests a theory of learning proposed as far back as 1949 by psychologist Donald Hebb, which posits that the sequential activation of neurons would strengthen the connection between them, while activity out of sequence would weaken the connection. Specifically, he states:

“When an axon of cell A is near enough to excite cell B repeatedly or persistently takes part in firing it, some growth process or metabolic change takes place in one or both cells such that A’s efficiency, as one of the cells firing B, is increased.”<sup>33</sup>

In STDP, a synapse is either potentiated or depressed based on the order of excitation of the two connected neurons, with the strength of the change dependent upon the length of the interstimulus interval. In hippocampal neurons, when presynaptic firing is followed repeatedly by postsynaptic firing (positive timing) long term potentiation (LTP) occurs, while in the reverse order of firing (negative timing), long term depression (LTD) occurs<sup>8, 18, 52</sup>.

Numerous experimental protocols have been used to elicit LTP and LTD at the CA3-CA1 synapse<sup>85</sup>. Although both LTP and LTD rely on  $Ca^{++}$  entry through NMDA receptors, protocols used to induce LTP classically involve high frequency stimulation, leading to a faster, higher

volume of  $\text{Ca}^{++}$  influx, compared to experimental protocols used to induce LTD (0.5-5 Hz)<sup>53</sup>. In the case of spike timing dependent plasticity (STDP), positive timing allows the synaptic cleft to be flooded with glutamate before backpropagating action potentials in the postsynaptic dendrites cause voltage-dependent relief of the  $\text{Mg}^{++}$  blocking the NMDA receptor channel<sup>47, 51</sup>. The coincidence of these two events allows maximal  $\text{Ca}^{++}$  influx. This  $\text{Ca}^{++}$  influx is believed to signal downstream cascades leading to the expression of LTP. In the case of negative timing, postsynaptic depolarization precedes presynaptic release, so the  $\text{Mg}^{++}$ -unblock is past its peak by the time glutamate binding takes place, and therefore  $\text{Ca}^{++}$  influx is not as large. This condition leads to LTD. This dichotomy based on the level of  $\text{Ca}^{++}$  is further supported by the correlation between the presynaptic-postsynaptic time interval, and magnitude of LTP or LTD induced<sup>8,9</sup>.

Backpropagating action potentials comprise the primary feedback signal to the synapse during STDP<sup>47</sup>. Some of these synapses can be a few hundred microns away, and the signal can attenuate during backpropagation<sup>79, 84</sup>. The amount of postsynaptic depolarization can be bolstered by local dendritic spikes. In pyramidal neurons, active currents at proximal locations are typically due to voltage gated sodium channels, while those at distal locations (hundreds of microns into the dendritic tree) are due to voltage gated calcium channels. Distally located synapses are also more likely to depend on dendritic spikes as a source of depolarization for plasticity<sup>37</sup>. In the case of CA1 pyramidal neurons, plasticity at synapses made by afferents from the entorhinal cortex, which form synapses in the outer regions of the dendritic tree (in the stratum lacunosum moleculare) are more likely to depend on dendritic spikes to provide depolarization to induce synaptic change, than CA3-CA1 synapses, which are located closer (within the stratum radiatum)<sup>158</sup>. The dendritic location of synaptic contact, therefore, can modulate STDP induction, and proximal synapses are more likely to exhibit fidelity to

conventional STDP rules of timing dependence<sup>26, 77, 78</sup>. Inhibitory synapses, made on the CA1 pyramidal neuron by interneurons, can also reduce backpropagating action potentials. It is important, therefore, to account for modulation by other synaptic inputs, in the design of STDP experiments.

### **1.3 INVESTIGATION OF HEBBIAN PROPERTIES USING EXOGENOUS APPLICATIONS OF GLUTAMATE**

The literature on LTP and LTD is vast and varied, with observations that implicate both presynaptic and postsynaptic changes in activity dependent potentiation and depression. Both LTP and LTD can be induced by presynaptically applied stimulation patterns, and the expression of LTP and LTD can be through increase or decrease, respectively, of presynaptic transmitter release<sup>80</sup>. However, it is also possible to induce synaptic change solely through postsynaptic manipulations. Induction of plasticity via exogenous applications of glutamate eliminates the role of presynaptic transmitter release, and allows one to narrow the field of possible induction mechanisms to those of postsynaptic origin. Although exogenous glutamate could activate presynaptic glutamate receptors, and induction of plasticity could activate retrograde endocannabinoid signaling<sup>23</sup>, if the postsynaptic current tested for LTP or LTD is in response to exogenously applied glutamate, then presynaptic changes in expression would not be detected in the potentiated or depressed current. A crucial benefit of using exogenously applied glutamate for induction and testing of plasticity, therefore, lies in the experimenter's ability to investigate postsynaptic mechanisms without conflation with results due to presynaptic induction or expression.

Attempts to induce LTP through photolytic uncaging of glutamate have sometimes resulted in induction of LTD instead<sup>24, 38</sup>. While these results may have implied an inability of postsynaptic membranes to potentiate in the absence of presynaptic stimulation, other methods, where glutamate was locally applied for several seconds, have induced LTP in hippocampal synapses<sup>15, 50</sup>. The scale of temporal precision in these methods, however, cannot be applied to investigate the Hebbian aspect of synaptic change, which relies on presynaptic and postsynaptic time differences of tens of milliseconds. More recently, two-photon uncaging of MNI-glutamate (specially formulated glutamate molecules) demonstrated timing dependent potentiation when small spines were specifically targeted for glutamate delivery<sup>56</sup>. The authors demonstrate that their method of uncaging glutamate mimics synaptic stimulation, by eliciting timing dependent structural changes in dendritic spines similar to that elicited by timing dependent potentiation through stimulation of Schaffer collateral afferents. The specificity of potentiation to a certain class of spines, along with further photolytic studies that succeed in potentiating glutamate responses on spines, but not on the dendritic shaft<sup>2</sup>, highlight the importance of location and precision of glutamate applied exogenously to elicit potentiation.

Two-photon uncaging of glutamate is an excellent method for rapid and highly localized delivery of glutamate over dimensions approaching 1  $\mu\text{m}$ , which is comparable to the size of individual synapses<sup>55</sup>. However, MNI-glutamate is so far the only caged neurotransmitter with a sufficient two-photon cross-section that has been successfully used to map the locations of glutamate receptors on hippocampal CA1 pyramidal neurons with such precision<sup>36</sup>. In order to probe postsynaptic mechanisms of STDP, it would be useful to have a technique, such as microiontophoresis, that can be extended to other agonists. Microiontophoresis is a technique whereby a controlled and constant rate of ions and charged molecules can be focally ejected in

very small amounts from glass micropipettes. This technique has been demonstrated to elicit glutamate responses similar to synaptic events in dissociated neuron cultures<sup>63, 77, 83, 84</sup>, and the technique can be easily extended from glutamate to similarly charged molecules, such as AMPA and NMDA. Iontophoresing through multibarrelled pipettes also allows simultaneous use of multiple agonists. This technique is efficient, accurate, and less costly than two-photon uncaging<sup>40</sup>. All of these advantages make microiontophoresis a good choice. Therefore, I explored whether it can be used to induce and study STDP in acute slice preparations.

## 2.0 MICROIONTOPHORESIS OF GLUTAMATE ON CA3-CA1 SYNAPSES

Popularly used for anatomically localized delivery of dye or pharmaceuticals *in vivo*, recent developments in instrumentation have refined microiontophoresis to the level of precision approaching synaptic events. Microiontophoresis simulating synaptic delivery of glutamate has been demonstrated in dissociated neuron cultures<sup>63, 77, 83, 84</sup>. Much of the seminal work in spike timing dependent plasticity was done in dissociated cultured neurons, and the basic principles of timing dependence as seen in these studies has been demonstrated in biologically wired neural circuits in organotypic and acute slice preparations, as well as in intact brains.

There is, however, no literature on millisecond level glutamate microiontophoresis in acute slice preparations. While individual synapses are easier to access in the dissociated culture preparation than in acute brain slices, cultured neurons grow in an artificial medium that does not replicate the cytoarchitecture, circuitry, glial environment, or excitatory-inhibitory balance that exist in the mammalian brain. Other factors, like synaptic strengths, distribution, proportion of receptor subunits, receptor colocalization, and dendritic properties may not be the same for neurons grown in culture and for neurons in brain tissue. Differences in experimental methodologies – such as the choice of experimental preparation, stimulation protocols, and chemicals used – can result in diverse and even contradictory claims about the conditions that lead to induction of STDP<sup>93</sup>. For example, in dissociated cell cultures, activation of a single excitatory neuron can trigger an action potential in a postsynaptic neuron via a single

suprathreshold EPSP<sup>9, 21</sup>. This is assumed not to occur in cortical circuits, since the average EPSP amplitude in pyramidal neurons is under 1 mV<sup>51, 53, 73</sup>. Such a difference may explain some discrepancies between STDP in cultured hippocampal neurons and at the CA3-CA1 synapse: LTP resulted reliably when presynaptic spikes occurred before postsynaptic spikes, but the same order of spikes at the CA3-CA1 synapse could result in LTP<sup>67</sup>, but in other cases result in LTD<sup>13</sup> or no plasticity<sup>70</sup>, likely due to insufficiently strong postsynaptic depolarization. Given the biological factors that are preserved in slice preparations to a greater degree than in dissociated cultures, accomplishing millisecond level glutamate microiontophoresis in a slice preparation is an important step in probing the postsynaptic mechanisms as pertinent to STDP in the brain.

## 2.1 MATERIALS AND METHODS

### 2.1.1 Microelectrodes for iontophoresis

The microiontophoresis system used for the experiments described here was designed following Murnick et al (2002)<sup>63</sup>, and refined by trial and error, guided by physical predictions and discussions on the nature of ionic transfer in *Microiontophoresis and Pressure Ejection* (1985) by T.W. Stone.<sup>83</sup> Pertinent details are discussed below.

My first attempt at fabricating iontophoresis electrodes emulated a protocol described by P. M. Lalley in “Modern Techniques in Neuroscience Research”<sup>41</sup>, a modified version of a method published in 1974<sup>16</sup>. Three borosilicate capillary tubes (O.D. = 1.0 mm, I.D. = 0.5 mm, length = 10 cm) with filaments were bundled together and bound with bands of heat-shrinkable

tubing, each band placed a few millimeters away from the ends of the tubes. This formed the 'blank', to be shaped into a multibarreled microelectrode on a vertical Narishige PE-2 puller. The blank was fixed in the chucks of the puller so that the ends were equidistant from the heating coil, and heated until the glass melted enough to stretch by gravity. After a short - a few millimeters – stretching of the glass, the lower half of the blank was quickly rotated through 270 degrees, and the heat turned off. After the glass cooled, a second round of heat was applied, this time accompanied by a magnetic pull adjusted to give two electrodes between 80 and 100 MΩ when filled with 150 mM glutamate. At the filling end of the pipette, the tubes were bent away from each other under heat, to avoid liquid bridges between the barrels.

Although adequate iontophoresis electrodes could be pulled in this manner, consecutive days of use at high heat settings led to changes in the shape of the heating coil, which led to inconsistencies in shape and resistance of the pulled electrodes. I therefore switched to a different method.

Electrodes used for iontophoresis, for all data in this document, were pulled in a single step on a Sutter P-97 Flaming/Brown horizontal puller programmed for heat and delay to give a tip size of less than 1 μm. Blanks used were purchased fused in triple barreled form, each tube consisting of borosilicate glass with filaments. Since the tubes were fused together all the way to the end, the filling ends could not be bent away from each other. Therefore, special care was taken during filling the pipettes, to avoid solutions spilling into an adjoining barrel. For all experiments shown, one of the three barrels was filled with 150 mM glutamate (L-glutamic acid, pH balanced to 8.0 with NaOH).

For delivery of chemicals with great spatial precision, electrodes must have tips that are narrow enough to limit application to a micron level of dendritic surface. A small tip opening,

followed by a long and narrow tip shape, assists this goal, and also minimizes damage to the surrounding brain tissue when the electrode is inserted into the slice. The opening of the electrode must be large enough to allow fast ion efflux, but small enough that the solution to be iontophoresed does not leak out between applications. Tip size and shape will limit leakage by diffusion. Leak can be further controlled by application of a positive backing current, which will tend to prevent efflux of the agonist.

In selecting the best electrode fabrication protocol, all of these factors were taken into consideration. The greater the backing current, the more the area at the tip would be depleted of our expected concentration of agonist. This would influence the ionic gradient and concentration of agonist at the tip of the iontophoresis electrode, changing the resistance at the tip over time as ejection current pulses were delivered<sup>83</sup>. Therefore, it was important that the backing current was just enough to stop loss by diffusion, and that small tip size, long and narrow shank leading to the tip and high resistance be utilized to lower the need for backing current. Our best iontophoresis electrode pulling protocols resulted in resistances between 100 and 200 M $\Omega$  (when filled with 150 mM glutamate) and required 2 to 4 nA of backing current. Any leak of glutamate from the tip of the electrode, when immersed in the recording bath, could be detected by an increase in baseline noise and change in holding current of the neuron under whole cell voltage clamp, and if the leak could not be controlled with 10 nA or less of backing current, the electrode was discarded.

The MVCS-02 (NPI Electronics) apparatus provides a high-voltage current source for controlling iontophoresis where constant currents in the nanoampere or microampere range are needed. Our MVCS-02 has an output compliance of  $\pm 45$  V, and comes with positive feedback capacitance correction for resistances below 300 M $\Omega$ . This last feature made it possible for us to

deliver chemicals very quickly, in the millisecond and sub-millisecond range<sup>64</sup>. The higher the resistance of the electrode, the greater the time constant ( $\tau = RC$ ) to reach steady state current ejection. For resistances in the hundreds of  $M\Omega$ , Murnick et. al. (2002)<sup>63</sup> measured a time constant of approximately 200 ms, implying that the electrode capacitance was approximately 2 nF. Without the circuit set by our device, charging of the uncompensated stray capacitance would vastly slow ejection of chemicals from the pipette.

The MVCS-02 consists of two independent iontophoresis injection channels, each with a digital ten-turn potentiometer for ejecting (out of the electrode) or retaining (into the electrode) currents and capacity compensation, as well as digital current display, overrange LEDs and two switches for selection of the operating mode. Long cables run from the main MVCS-02 to the head stages, which are mounted close to the recording chamber, and smaller BNC connectors run from the iontophoresis electrode to the headstage. The current output is measured at the headstage, thus minimizing the length of wire, and resulting stray capacitance, from current output to electrode. The backing current was set manually, and all stimulus waveform commands were applied through the computer using pClamp 9.2 (Axon Instruments, CA) and the analog output of a Digidata 1200B (Axon Instruments, CA). The current monitor of the MVCS-02 was connected to an analog input of the Digidata 1200B and acquired using pClamp 9.2.

Two steps were performed for every iontophoresis electrode, to protect against instability in iontophoretic current during the experimental period. First, when the iontophoresis electrode was lowered into the recording chamber bath, a -100 nA ejecting current was passed for 500 ms every 2 seconds. This was repeated for several minutes while monitoring the voltage response to the current being passed through the iontophoresis electrode. This was done to rid the tip of air

bubbles. The voltage response changed from trial to trial until all bubbles had been cleared. Once a stable voltage response was elicited, the test was repeated for a few minutes more to ensure that the responses remained stable. The test pulse was then reduced to -10 nA, and the electrode was lowered further into the bath, and placed just above the tissue slice. Capacitance correction was applied after a steady state response had been reached, and the backing current applied such that the current monitor displayed a holding current greater than zero. Neurons with dendrites close to the surface (within 10 or 20  $\mu\text{m}$  below the surface) were selected, and no further capacitance compensation was necessary after insertion of the iontophoresis tip into the slice. The second step performed to protect against instability in iontophoretic current was monitoring of the voltage response at the of the iontophoresis electrode. For the same current pulse delivered at periodic intervals over several minutes, a change in the voltage response would indicate a change in ion exchange through the iontophoresis electrode. All experimental trials included steady monitoring of the iontophoretic voltage response to ejection current, and if the voltage response changed by more than 2% during the trial, the results were discarded. Clogging events, seen in early trials, were characterized by noticeable changes in voltage response, followed by large ejection of glutamate (as seen by the neuron's response). When glutamate was regularly filtered before use and the above mentioned precautions were followed before starting an experiment, clogging problems were rare.

The MVCS-02 also comes with a balance module that can reduce artifacts caused by the iontophoretic drug application by applying, through an additional electrode, an equal but inverted sum of current output supplied by the iontophoresis channels. Since the artifact did not occlude my measurements of glutamate evoked current, I did not use the compensation channel in my experiments.

### 2.1.2 Slice preparation and Electrophysiology

Hippocampal slices were prepared from young Sprague-Dawley rats (postnatal day 14-22). Animals were injected with 0.3 ml. of 8% chloral hydrate, decapitated and brains removed in chilled ACSF with a high concentration of  $Mg^{++}$  (4 mM). The best slices for study were those which had healthy neurons near the surface of the slice, with apical dendrites that were intact and could be detected continuously for at least 150  $\mu m$  away from the soma. We found that horizontal sections of the hippocampus obtained by tilting each cerebral hemisphere laterally, while sectioning, gave the best slices. In order to accomplish this, I removed the brain from the animal, removed the cerebellum and frontal third of the cerebrum with a coronal cut, then placed the brain on its rostral end, and cut and discarded a ventrolateral section from each of the hemispheres at a 20° angle from the ventral surface. The hemispheres were then separated and affixed to the slicing chamber on their ventrolateral surface, thus resulting in a lateral tilt of the hemispheres containing the hippocampal region. Slices were cut at a thickness of 350  $\mu m$  in a chamber, filled with ice-cold high  $Mg^{++}$  ACSF, on a Leica VT1000 S (Leica Microsystems) vibrating microtome. For some trials, a Vibratome 1000 (Ted Pella, Inc.) was used. Slices were incubated in regular ACSF at 36°C for 40 minutes, then transferred to room temperature, with a total incubation time of at least an hour before being transferred to recording chamber for use.

Pyramidal neurons in the CA1 region were visualized under infra-red DIC microscopy on an upright Axioskop (Carl Zeiss Microimaging Inc.) on a computer screen through a digital CCD CoolSNAP (Roper Scientific Inc.) camera driven by IPLab software (BD Biosciences Bioimaging, MD). A pyramidal neuron was selected, and the slice was positioned such that the the main trunk of the apical dendrite of the selected neuron extended diagonally across the viewing surface, as shown in **Figure 1 (a)**. The iontophoresis electrode, which was held with a

positive backing current to protect against agonist leak, was positioned with its tip close to the main trunk of the apical dendrite. Dendritic distance from the soma was measured from the point of initiation of the dendrite. The recording electrode was then lowered to the neuron, and whole cell clamp achieved. **Figure 1 (a)** shows the lateral approach of the tip of the iontophoresis electrode. Some fine axial movement of the tip was undertaken before data were collected, to decide on the optimal tip position. This movement did not affect the tip's distance from the soma as measured along the dendrite.

Electrodes used for whole cell recording were between 5-8 M $\Omega$ , and contained cesium to facilitate voltage control across the entire neuron. After whole cell configuration was achieved, the cell was clamped at  $V_m = -59$  mV (after junction potential correction) except where noted otherwise. The whole cell response to glutamate iontophoresis observed for an iontophoretic current of 5 ms was used to gauge distance from a responsive region of dendrite. If I saw a delay in onset of the response, I moved the iontophoresis tip closer to the dendrite. The goal was to reduce onset latency as much as possible, with the shortest possible duration of iontophoretic current ( $I_{\text{iont}}$ ) that consistently elicits a response from the neuron. In some cases, a larger  $I_{\text{iont}}$  was used to get a larger evoked response. The amplitude and duration of  $I_{\text{iont}}$  decided at this time was used for the course of the experiment as test pulses, as well as for iontophoresis during the plasticity induction protocol. All iontophoretic current pulses were commanded through the computer and measured by the current monitor. The amplitude of the iontophoretic current used for experiments ranged between -50 to -400 nA.

High  $\text{Mg}^{++}$  ACSF used for slicing contained the following (in mM): 1.9 KCL, 1.2  $\text{Na}_2\text{HPO}_4 \cdot 7\text{H}_2\text{O}$ , 33.34  $\text{NaHCO}_3$ , 10 Glucose, 4  $\text{MgCl}_2 \cdot 7\text{H}_2\text{O}$ , 1  $\text{CaCl}_2$ , 220 Sucrose (310 mOsm, pH 7.4). Regular ACSF used for incubation of slices and recordings contained the following (in

mM): 125 NaCl, 2.5 KCl, 25 Glucose, 2 CaCl<sub>2</sub>·H<sub>2</sub>O, 1 MgCl<sub>2</sub>·6H<sub>2</sub>O, 1.25 NaH<sub>2</sub>PO<sub>4</sub>, 25 NaHCO<sub>3</sub>, Sucrose (310 mOsm, pH 7.4). 0 Mg<sup>++</sup> ACSF used for a few experiments contained all the same ingredients as regular ACSF, except MgCl<sub>2</sub>·6H<sub>2</sub>O. TTX (1 μM), NBQX (10 μM), APV (50 μM) were purchased from Sigma-RBI. Intracellular whole cell pipette solution contained the following (in mM): 122.5 Gluconic Acid, 122.5 CsOH, 17.5 CsCl, 10 HEPES, 0.2 EGTA, 8 NaCl (295 mOsm, pH 7.2). Iontophoresis pipette solution consisted of 150 mM L-glutamic acid, pH balanced to 8.0 with NaOH.

Recordings were done in regular ACSF (unless otherwise mentioned) perfused at the rate of 2 ml/min through a peristaltic pump, at 30°C. TTX (1 μM) is added to all recording solutions to block regenerative Na<sup>+</sup> currents. Junction potential between intracellular and extracellular solutions were measured and correction (-11 mV) was applied post hoc. Series resistance was less than 30 MΩ, and was checked before and after experiment to ensure no change. Holding currents were less than -300 pA. Input resistance was calculated by measuring the current response to a rectangular 5 mV hyperpolarizing pulse applied at the beginning of every trial. Data were accepted for analysis if the following criteria were met: Neither input resistance nor holding current change more than 35%, as averaged over 5 minutes, from beginning to end of the experiment; if there was drift in pipette voltage before and after experiment, it was less than 2 mV; voltage response the iontophoresis pipette, as recorded during iontophoretic glutamate ejection, did not change more than 2%.

Data were acquired through a Digidata 1200B (Axon Instruments, CA) and Axopatch 200B patch clamp amplifier (Axon Instruments, CA) at a sampling rate of 10 kHz, output gain 10x, lowpass Bessel filtered at 5 kHz, monitored online and saved for offline analysis through pClamp 9.2 (Axon Instruments, CA). Throughout this document, the stated amplitude of the

iontophoretic current is as commanded. The iontophoretic current as measured through the current monitor is seen to be slightly less than command for short (few ms or less) pulse durations, by a fraction that becomes significantly larger for command amplitudes of 300 nA and more. The final outcome of each STDP experiment was calculated from mean glutamate evoked current amplitude 15-20 minutes after induction protocol, and is expressed as mean  $\pm$  S.E.M. Two tailed t-test was used to evaluate significance. Linear regression was used to analyze correlations between parameters. Analysis was done on Clampfit 9.2 (Axon Instruments, CA) and Origin 7.0 (OriginLab Corp, MA).

### **3.0 RESULTS**

Micropipettes were fabricated for submillisecond iontophoresis of glutamate on dendritic receptors involved in synaptic transmission and plasticity at CA3-CA1 synapses in acutely prepared hippocampal brain slices. The CA1 pyramidal neuron's response to the iontophored glutamate was then examined. My goal was to develop a system of glutamate delivery that affects dendritic receptors locally, with a precisely controlled and reliably reproducible technique capable of evoking a neuronal response to the iontophored glutamate on the timescale of milliseconds. This technique was then evaluated for the ability to induce timing dependent plasticity, and its utility in the study of postsynaptic mechanisms of STDP independent of presynaptic change.

#### **3.1 CHARACTERIZATION OF CA1 PYRAMIDAL CELL RESPONSES TO GLUTAMATE IONTOPHORESIS**

All recordings were done from CA1 pyramidal neurons under whole cell voltage clamp, and responses were evoked by iontophoresis of glutamate at the dendrite of the neuron after whole cell configuration was achieved.

**Figure 1(a)** shows an example of the iontophoresis electrode at the dendrite of the neuron. In this example, the tip of the iontophoresis electrode is 60  $\mu\text{m}$  away from the soma. **Figure 1(b), Left**, shows inward current elicited by iontophoresis of glutamate. The neuron is held at membrane potential ( $V_m$ ) of -70 mV in regular ACSF, with TTX (1  $\mu\text{M}$ ) to inhibit polysynaptic currents or action potentials. The iontophoretic current ( $I_{\text{iont}}$ ) is -100 nA, programmed to be delivered for 0.5 ms. Addition of NBQX (10  $\mu\text{M}$ ) to the extracellular recording solution eliminated the current, confirming that it was an AMPA receptor mediated current. In order to unmask an NMDA mediated component that may also be activated by the  $I_{\text{iont}}$ , but might be blocked by  $\text{Mg}^{++}$  in the extracellular recording solution, I perfused the recording bath with ACSF that was constituted without any  $\text{Mg}^{++}$  (0  $\text{Mg}^{++}$  ACSF), with NBQX (10  $\mu\text{M}$ ) added, to continue inhibiting the AMPA receptors. Several minutes after the recording chamber should have filled with 0  $\text{Mg}^{++}$  ACSF, no glutamate evoked current was visible. When I increased the duration of the iontophoretic current from 0.5 ms to 1 ms, I saw a glutamate evoked current (**Figure 1(b), Right**). This current increased in size when the amplitude of the iontophoretic current was increased. The duration of the iontophoretic current was maintained at 1 ms. When the amplitude of  $I_{\text{iont}}$  was increased to -250 nA, to elicit a response similar in amplitude to the AMPA current seen before, the evoked current exhibited a much larger half-width, 20% to 80% rise time and 80%-20% decay time than that observed for the AMPA current, which matched my expectations for an NMDA mediated current. The evoked current was no longer visible when APV (50  $\mu\text{M}$ ) was added to the extracellular bath solution, confirming that it was an NMDA receptor mediated current. The kinetics of the currents observed under each set of conditions were averaged over two minutes of responses recorded at the rate of 6 per minute, and are shown in **Table 1**. As  $I_{\text{iont}}$  amplitude was increased, the half-width and decay time of the

NMDA current increased (73% and 22% respectively) much more than its rise time (no significant increase). This could be due to glutamate spreading to farther receptors for the larger iontophoretic current.

When the amplitude of the iontophoretic current was increased from -100 nA to -200 nA, the half-width and decay time of the AMPA current only increased by 16% and 13% respectively, unlike the NMDA current shown in **Figure 1 (b)**, which increased by much greater proportions (73% and 22%, respectively). This measurement cannot be directly ascribed to a difference between AMPA and NMDA currents, since the duration of iontophoresis differs between the two experimental conditions, and other conditions, such as distance of iontophoretic electrode from the receptors, density of receptors and properties of receptor responsiveness may differ in ways that I am not measuring. However, I could frequently evoke AMPA currents by  $I_{\text{iont}}$  that was programmed to be a fraction of a millisecond in duration, often as small as 0.1 ms, while NMDA currents could not ever be evoked by iontophoresing for less than 1 ms, even when the same iontophoresis electrode was used, and not moved in between evoking AMPA and NMDA responses, and therefore, presumed to be at the same location relative to the postsynaptic sites. This may be due to incomplete removal of  $\text{Mg}^{++}$  from the NMDA receptors, even though the recordings were done in 0  $\text{Mg}^{++}$  ACSF. Even after the recording chamber had been perfused with 0  $\text{Mg}^{++}$  ACSF for 10 minutes, depolarizing the neuron causes an increase in amplitude of the NMDA mediated current, suggesting that there was still some  $\text{Mg}^{++}$  block at resting potential (data not shown).

While I could place the iontophoresis electrode close to the dendritic membrane visually, as seen in the **Figure 1(a)**, I could get even closer by using the glutamate response as a guide. This movement is on the level of microns, however – I could not see the tip of the electrode

move, even as I commanded movement forward or backward along the axis of the iontophoresis electrode through the pipette manipulator. The change in glutamate evoked current ( $I_{\text{iont}} = -50$  nA, for 1 ms.) in a neuron in regular ACSF, with TTX (1  $\mu\text{M}$ ), in response to micron level movement of the tip of the iontophoresis electrode is shown in **Figure 1(c)**. It was expected that a movement of the iontophoresis electrode would change the onset latency of the evoked current, but the data do not support this expectation.

**Figure 2(a)** displays responses from a neuron, with the iontophoresis electrode 100  $\mu\text{m}$  away from the soma, in regular ACSF with TTX (1  $\mu\text{M}$ ). The amplitude of  $I_{\text{iont}}$  was progressively increased to see the effect of different amplitudes of iontophoretic current on the evoked response. All iontophoretic pulses were 0.1 ms in duration. Single current responses were measured in response to each  $I_{\text{iont}}$  amplitude level, sequentially recorded, and are shown in **Table 2**. The time it took for the evoked currents to reach peak amplitude changed as the iontophoretic current amplitude was increased, but the latency to onset of evoked current did not change notably.

Another interesting observation was the grouping, rather than a smooth gradation, of response size as the  $I_{\text{iont}}$  amplitude is increased. When the amplitude of the command  $I_{\text{iont}}$  was increased from -100 nA to -200 nA, there was an increase of 140.5 pA in peak response amplitude. However, when the amplitude of command  $I_{\text{iont}}$  was raised by 100 nA for further trials, the increase in peak response amplitude was only a few tens of pA. On checking the actual change in iontophoretic current, through the current monitor, I found it was 3% less than the current as commanded at values -80 nA, -100 nA, -200 nA, and 1.5% less than the command current at -300 nA. However, there was a 12% loss when commanded current was -400 nA, and 28% loss when commanded current was -500 nA. Even though the iontophoresis current source

did not reach its saturating voltage, the electrode was not able to deliver my choice of current for larger amplitudes, possibly because the capacitance was too large to be fully charged within 0.1 ms. For smaller iontophoretic currents, (upto -300 nA) the current monitored is more accurately representative of the command current. The glutamate evoked responses changed fairly linearly as a function of measured (through current monitor) iontophoretic current (**Figure 2(b)**) upto  $\sim -200$  nA. For higher iontophoretic currents, the receptors may be nearing saturation.

It was important that the glutamate evoked response was reliable over at least a few tens of minutes, if I were to use this method to investigate STDP. **Figure 3** shows the peak amplitude of responses elicited and recorded at the rate of 3 per minute ( $I_{\text{iont}} = -200$  nA, for 0.1 ms) at a single dendritic site 100  $\mu\text{m}$  away from the soma, with TTX (1  $\mu\text{M}$ ) present in the extracellular ACSF. When responses were elicited at this rate, no net rundown or sensitization was seen.

Although the iontophoresis evoked responses shown so far were all done in the presence of TTX, the use of TTX in my experiments was not a simple decision. TTX blocks  $\text{Na}^+$  channels, which are activated by the depolarization of the dendritic membrane in response to glutamate. Influx of  $\text{Na}^+$  depolarizes the membrane, and membrane voltage can quickly exceed the threshold for action potential generation. In CA1 pyramidal neurons receiving synaptic input from axons of CA3 neurons, the summation of synaptic depolarization generates action potentials at the axon hillock which backpropagate along the dendrites, and are believed to be very important in voltage-dependent relief of  $\text{Mg}^{++}$  block of the NMDA receptor channel while the synaptic cleft is flooded with presynaptically released glutamate<sup>31, 47, 51</sup>. In the absence of action potentials, the fast and large  $\text{Ca}^{++}$  influx believed to be essential for LTP induction, resulting from the spike timing dependent coincidence of depolarization and glutamate available

for binding, may not occur. In that case, using TTX in my extracellular solution would have inhibited my ability to reproduce STDP through glutamate iontophoresis.

However, when I recorded iontophoresis events in regular ACSF without TTX, the iontophored glutamate caused enough depolarization for the  $\text{Na}^+$  currents to exceed threshold. **Figure 4** shows spikes that were generated on the glutamate evoked response. I used  $\text{Cs}^+$  in my whole cell recording pipette solution, instead of  $\text{K}^+$ , which blocks  $\text{K}^+$  channels and improves voltage control across the neuron; however, it also makes the resting membrane potential in the dendrites closer to 0 than when  $\text{K}^+$  is used in the pipette, and more likely to develop  $\text{Na}^+$  spikes at poorly clamped dendrites. The spikes were narrower than dendritic spikes generally are, most likely because the voltage clamp compensated quickly after the emergence of the fast  $\text{Na}^+$  depolarization.

Even when  $I_{\text{iont}}$  was adjusted to a level such that spikes were not activated (first 5 minutes of **Figure 4(b)**), application of a positive depolarization-iontophoresis pairing protocol (D-I protocol: explained in *Section 2.2.3*) led to conversion of the passive glutamate responses to responses tainted with  $\text{Na}^+$  spikes. While this result favored the idea that the D-I protocol increased some aspect of postsynaptic excitability, the spikes were larger than -800 pA, saturating the digitizer, so I could not measure the peak response. Additionally, I could not quantify the change in AMPA mediated response to glutamate iontophoresis. Following a few experiments that exhibited similar behavior, I decided to use TTX in the extracellular recording solution for all experiments. The depolarization that would have been provided by active  $\text{Na}^+$  currents was instead provided by a rectangular depolarizing pulse, through the voltage clamp. The site of iontophoresis is 100  $\mu\text{m}$  away, which allows reasonably good voltage control from

the soma<sup>34, 12, 28</sup>. The depolarization pulse is 4 ms long, and depolarizes to +11 mV, to compensate for the slight degradation of the commanded voltage down the passive dendrite.

### **3.2 EXPLORATION OF A PARAMETER SPACE FOR IONTOPHORETICALLY INDUCED STDP**

Spike timing dependent plasticity (STDP) induces a change in synaptic strength through relatively timed activity of the two neurons forming the synapse. Nomenclature of relative timing adopted in STDP literature refer to “positive” and “negative” pairings: a presynaptic event paired with a postsynaptic event that follows, is said to have occurred with a positive time interval (pre- before post-) whereas the reverse (post- before pre-) pairing is said to have occurred with a negative time interval. In my technique, using iontophoresis as the source of glutamate for the dendritic AMPA receptors, there was no presynaptic release of glutamate. My protocol for investigating induction of LTP or LTD mimics the standard STDP concept, and pairs glutamate iontophoresis with depolarization of the neuron whose dendrites are targeted for iontophoresis. In this document, I refer to this as the depolarization-iontophoresis pairing protocol (D-I protocol). Two D-I protocols were designed, and one of these two were used for each of the subsequent experiments: a positive D-I, where  $I_{\text{iont}}$  began 10 ms before the depolarization of the neuron began (+10 ms time interval), and a negative D-I, where the depolarization of the neuron began 10 ms before  $I_{\text{iont}}$  began (-10 ms time interval). During the D-I protocol, each pairing of depolarization and iontophoresis was done at the rate of 5 Hz for 20 seconds. Each depolarization was a rectangular pulse that clamped the neuron for 4 ms at +11 mV.

At the beginning of the experiment, glutamate was iontophoresed, and AMPA mediated response of the neuron noted through the whole cell recording electrode, to decide upon an amplitude and duration of  $I_{\text{iont}}$  that would be used. Slight adjustment to the position of the tip of the iontophoresis electrode may have been made to reduce onset latency as much as possible. The shortest possible duration of  $I_{\text{iont}}$  that consistently elicited a response from the neuron was noted. This adjustment of the tip did not change the iontophoresis electrode's distance from the soma, which was maintained at 100  $\mu\text{m}$ . The amplitude and duration of this  $I_{\text{iont}}$ , or an amplitude slightly larger, was then selected for use and was used in the experiment, for test pulses as well as for iontophoresis during the D-I protocol.

In all positive D-I experiments, test pulses were delivered, and glutamate evoked response recorded, once every 20 seconds. In all negative D-I experiments, test pulses were delivered, and glutamate evoked response recorded, once every 10 seconds. This was done so that a larger number of responses could be averaged per minute, to reduce the effects of variation due to noise. During preliminary experiments, the rate of events per minute were increased in the negative D-I set after it was assessed that consecutive test pulses delivered once every 10 seconds did not lead to sensitization or attenuation of consecutive trials, the same as when test pulses were delivered once every 20 seconds. After necessary parameters for successful, deterministic STDP induction was established, future experiments would have been done with test pulses delivered once every 10 seconds. All other elements of experimental design, cell selection, rejection criteria and analysis methods remained same between positive D-I and negative D-I datasets.

**Figure 5** is an example of the change in peak amplitude of the glutamate evoked current that occurred in one positive D-I pairing experiment. The time when D-I protocol was applied is

marked with the solid red arrow. Each data point plotted for peak amplitude is from an average of three consecutive evoked currents. Final peak amplitude ( $95.9 \pm 4.5$  pA) was 19.3% greater than the average peak amplitude during the initial 5 minute baseline ( $80.4 \pm 6.1$  pA). The 20% to 80% rise time did not change much over time ( $r = 0.04$ ,  $p = 0.81$ ), or vary with peak amplitude ( $r = -0.03$ ,  $p = 0.86$ ). Onset latency did not drift over time ( $r = -0.33$ ,  $p = 0.06$ ) or vary with peak amplitude ( $r = -0.23$ ,  $p = 0.17$ ), so I do not suspect the observation of greater peak amplitude to be due to movement of the iontophoresis pipette. Additionally, since the iontophoresis tip was positioned, at the beginning of the experiment, where test pulses elicited maximal response, any drift in the electrode (unless it is to a completely different set of dendritic receptors) should have caused a decrease, not increase, in the amplitude of glutamate response. In all experiments that resulted in LTP, increase in amplitude occurred around 10 minutes after the induction protocol, and onset latency did not correlate to the increase in peak amplitude ( $r^2 < 0.33$ ).

Only 5 out of 9 experiments subjected to positive D-I pairing showed potentiation of the evoked response. The other 4 showed depression following the same D-I pairing protocol. **Figure 6** is an example of decrease in peak amplitude of the glutamate evoked current following a positive D-I pairing induction protocol. The final peak amplitude ( $42.1 \pm 3.1$  pA) was 57.9% decreased from the average peak amplitude during the initial 5 minute baseline ( $100.1 \pm 5.2$  pA). In the post-induction period, as the size of the evoked currents got smaller, their shape changed considerably as well. Measures of onset latency and time of peak were not easily differentiable from noise. This was seen consistently in positive D-I experiments that led to depression of the glutamate evoked response; in some cases, the response reduced to being barely distinguishable from noise. The measurements taken, despite these limitations in accuracy, reveal that the 20% to 80% rise time increased with time ( $r = 0.72$ ,  $p < 0.0001$ ), as peak amplitude grew smaller ( $r =$

-0.65,  $p < 0.0001$ ), although onset latency was not correlated with time ( $r = 0.55$ ,  $p = 0.001$ ) or peak amplitude change ( $r = -0.49$ ,  $p = 0.006$ ) as much. The challenge of monitoring onset latency, and possible implications, are discussed later in more detail. In all positive D-I experiments that resulted in LTD, onset latency did not correlate to the decrease in peak amplitude ( $r^2 < 0.39$ ).

The negative D-I protocol resulted in LTD for all 4 of the experiments. An example of a negative D-I pairing experiment is shown in **Figure 7**, where the final peak amplitude ( $1.2 \pm 0.3$  pA) was 96.5% decreased from the average peak amplitude during the initial 5 minute baseline ( $34.7 \pm 1.6$  pA). 20% to 80% rise time did not increase with time ( $r = -0.25641$ ,  $p = 0.14325$ ) or peak amplitude ( $r = 0.04534$ ,  $p = 0.79901$ ). Similar to the depression seen in response to some of the positive D-I experiments, responses reduced drastically, with signal to noise ratio decreasing too much to get reliable measures of onset latency or peak time. In all 4 of the negative D-I pairing experiments, the response depressed to being barely distinguishable from noise.

A total of 13 experiments are summarized in **Figure 8**. Positive pairing ( $n = 9$ , black triangles) and negative pairing ( $n = 4$ , blue triangles) are presented. Outcomes were compared to changes in holding current (positive pairings:  $r = -0.4$ ,  $p = 0.30$ ; negative pairings:  $r = 0.2$ ,  $p = 0.80$ ) and input resistance (positive pairings:  $r = -0.6$ ,  $p = 0.09$ ; negative pairings:  $r = 0.5$ ,  $p = 0.46$ ). While the positive pairing experiments did not result in any net change in peak amplitude from the initial baseline period (mean change:  $-8.2 \pm 23.0$  %), the negative pairing experiments showed LTD (mean change:  $-85.7 \pm 7.7$  %). The two groups are not significantly different (Two sample t-test,  $p = 0.053$ ).

Why do some positive pairing induction protocols result in LTP, while others result in LTD, with no apparent bias towards either outcome? Perhaps the difference in experimental outcome is influenced by initial conditions. Initial conditions were analysed for correlation to the outcome of positive pairing experiments (**Figure 9**). The percent change in amplitude of glutamate evoked response was analysed as a function of peak amplitude (**Figure 9(a)**) and half-width (**Figure 9(b)**) of initial baseline responses, and age of the animal (**Figure 9(c)**) from which slices were taken. Both amplitude and half-width could be controlled by the amount of glutamate iontophoresis, and could perhaps reflect spread of glutamate. The initial amplitude correlated strongly with negative percent change ( $r = -0.80$ ,  $p = 0.01$ ); transitioning around a mid-point of 100 pA, the smaller the current, the more likely they seemed to potentiate, and the larger the current, the more likely they seemed to depress. The initial half-width did not show a correlation to percent change in current ( $r = -0.08$ ,  $p = 0.83$ ). The age of the animal shows a bias towards decrease in amplitude at younger ages, but the correlation is not significant ( $r = 0.62$ ,  $p = 0.07$ ). A total of  $n = 9$  positive pairing experiments are analyzed for initial conditions; it is possible that the trend seen in **Figure 9(c)** would have reached significance for a larger sample size.

Assuming that the initial size of glutamate evoked response was an important determinant of size and direction of plasticity, the positive pairing experiments were split into two groups: one for all trials where average initial evoked response was less than 90 pA, and another where the average initial evoked response was greater than 90 pA. These two groups are summarized in **Figure 10(a)**. The group with smaller ( $<90$ ) initial current amplitudes ( $n = 4$ ) showed potentiation, with mean percent increase of  $48.9 \pm 15.8\%$ , while the group with larger ( $>90$ ) current amplitudes ( $n = 5$ ) showed depression, with mean percent decrease of  $53.8 \pm 24.1$ . The

outcomes were significantly different (Two sample t-test,  $p = 0.012$ ). The time course of depression seen for the  $<90$  positive pairings was similar to the time course of depression seen for negative D-I pairings (**Figure 10(b)**). It appears that positive D-I pairings would result in LTP if the initial amplitude of glutamate evoked current was less than 90 pA. All negative D-I pairings, already summarized in **Figure 8**, had initial amplitudes less than 90 pA and resulted in LTD. It is possible, then, if I only focused on currents with initial amplitude of less than 90 pA, positive D-I pairings would have lead to LTP and negative D-I pairings lead to LTD. All experiments with initial peak amplitude less than 90 pA are summarized in **Figure 10(c)**. Outcomes were significantly different for positive and negative D-I pairings (Two sample t-test,  $p = 0.00026$ ).

What was characteristically different for larger amplitude currents? One possibility was that larger currents have a later time of reaching their peak amplitude, and therefore were not experiencing the same depolarization-iontophoresis time interval as smaller currents. The positive D-I protocols were designed with the expectation that, in each pairing, the dendritic membrane would be depolarized close to the time of peak glutamate evoked current. The time from beginning of the iontophoretic current, to the beginning of the depolarization, was 10 ms. However, if the evoked current did not reach its peak within 10 ms, the depolarization would have begun before the glutamate peak current. The depolarization pulse is 4 ms long; for currents that reached their peak more than 14 ms after the beginning of the iontophoretic pulse, the depolarization was over by the time the glutamate evoked current peaked. The postsynaptic depolarization, in that case, occurred earlier than maximum glutamate binding. This measurement of the time interval is illustrated in **Figure 11(a)**, and **Figure 11(b)** shows a plot of experimental outcome as a function of time difference ( $\Delta t$ ) between the mid-point of

postsynaptic depolarization (since the depolarization lasts for 4 ms) and peak glutamate current. All experiments ( $n = 13$ ), positive as well as negative D-I pairings, are shown. The insets to the right of the plot show sample currents from the initial baselines, overlaid with the current trace showing the time of depolarization. In first sample current, corresponding to datapoint at  $\Delta t = -16.1$  ms, Percent Change =  $-88.7$ , the depolarization is over before the evoked glutamate current reaches peak amplitude. In contrast, in the third sample current, corresponding to datapoint at  $\Delta t = -4.4$  ms, Percent Change =  $+58.6$ , the depolarization coincided with the peak glutamate current. Not all LTP/LTD events could be accounted for by the time interval calculated in this way. Initial amplitude of evoked currents does not correlate to  $\Delta t$  ( $r = 0.12$ ,  $p = 0.77$ ). **Figure 11(b)** shows depression for some of the events (initial currents  $> 90$  pA) that were in the same  $\Delta t$  range as events that resulted in potentiation.

## 4.0 DISCUSSION

Preliminary data presented in this document suggests that microiontophoresis is a viable technique for induction of spike timing dependent plasticity without involvement of a presynaptic neuron. This is useful for isolation and study of the postsynaptic mechanisms involved in spike timing dependent plasticity.

### 4.1 SPATIAL AND ANATOMICAL ASPECTS

Early modeled predictions of density of spines on apical dendrites of CA1 neurons claimed that spine density peaked between 200 and 250  $\mu\text{m}$  from the soma, with an estimated density of 1 spine every 2.5  $\mu\text{m}$  of dendritic length at 100  $\mu\text{m}$  from the soma<sup>72</sup>. However, quantification of spines through morphometric analysis indicate that the soma and early regions of apical dendrites are free of spines, with spines starting to appear about 100  $\mu\text{m}$  away from the soma, followed by fairly regularly spaced spines at a density of 2-3 spines/micron<sup>1, 3, 30, 88</sup>. During iontophoresis in all experiments shown, I am eliciting responses from a few distinct synaptic sites, and extrasynaptic receptors in between them.

Fluorescence  $\text{Ca}^{++}$  imaging studies have demonstrated that  $\text{Ca}^{++}$  influx through NMDA receptors and voltage dependent  $\text{Ca}^{++}$  channels exhibit supralinear summation in STDP

experiments where presynaptic spiking was followed by postsynaptic spiking, and sublinear summation where the order of spikes was reversed<sup>17, 39, 65</sup>. A relative timing relationship may be characterized in terms of the observed EPSC, which is mostly an AMPA mediated response, but it is the relative timing with respect to NMDA mediated currents that directly affects  $\text{Ca}^{++}$  influx. In my experiments, I measured  $\Delta t$  with respect to AMPA currents, which may be used to infer associated NMDA activation times.

The lifetime of synaptically released glutamate within the synaptic cleft of adult rat hippocampal synapses is  $\sim 1$  ms<sup>14, 19, 20</sup>. The rate of glutamate uptake is five times slower in rats that are 12 – 14 days old (P12-14)<sup>20</sup>. Synaptically released glutamate is delivered directly into the cleft, whereas iontophoretically released glutamate takes longer to reach the cleft. It is likely to produce a slow rise in glutamate concentration in the cleft, compared to synaptically released glutamate; this would be even slower for receptors that are distant from the tip of the iontophoresis microelectrode. Jeffrey Diamond (2005)<sup>20</sup> found that time course of glutamate clearance by glial transporters was not affected by afferent stimulus strength or release probability. He also found that synaptically released glutamate was taken up at the same rate as glutamate released via flash photolysis, indicating that the spatial location of glutamate release relative to presynaptic membrane did not affect the time course of clearance. The time course of clearance was also unaffected by the amount of glutamate uncaged. I assumed, therefore, that the spread of glutamate delivered through microiontophoresis would be comparable to that modeled by Diamond (2005)<sup>20</sup>. This model considered the diffusion of glutamate to neighboring regions, limited by the rate of glutamate uptake, and adjusted for extracellular concentration, neuropil barriers, and an assumed temperature of 35°C. According to the model, in adult (> P60) glia, the majority of glutamate molecules do not spread more than 1  $\mu\text{m}$  (linear distance,  $0.89 \pm$

0.58  $\mu\text{m}$ ) away from the point of release, while in P12-14 glia, glutamate spreads about twice as far ( $1.7 \pm 1.2 \mu\text{m}$ ).

In my experiments, slices were made from animals aged P14-P20, and maintained at 30°C while recording. Assuming some uncertainty due to these deviations from Diamond's simulated conditions, I estimated that the distance traveled by glutamate molecules released by iontophoresis, in slices taken from P14 animals, was 1.7  $\mu\text{m}$ . The maximum possible area covered by glutamate spread, then, would be over a circular area:  $\pi (1.7)^2 = 9.1 \text{ sq. } \mu\text{m}$ . Even if the dendrite was 2  $\mu\text{m}$  in diameter<sup>3</sup>, much of the spreading glutamate would diffuse past the dendrite. Instead, using the average of 2.5 spines/ $\mu\text{m}$ <sup>1, 3, 30, 88</sup> along the length of a dendrite, and assuming bidirectional diffusion from the iontophoretic tip, I assess that iontophoresis of sub-microsecond duration had the potential to elicit response from:  $2 \times 1.7 \times 2.5 = 8.5$  spines.

## 4.2 FACTORS AFFECTING INDUCTION OF LTP VERSUS LTD

Positive pairing of iontophoresis with depolarization to induce STDP resulted in a bias towards LTD when larger glutamate evoked currents were used. It has been previously reported that the amount of LTP is inversely correlated with the initial synaptic strength<sup>8, 39, 42, 78</sup>. Larger postsynaptic currents were less likely to potentiate, in these studies, which appears similar to my observations in **Figure 9(a)**. However, synaptically evoked glutamate responses are shaped not only by postsynaptic receptors, but also by the features particular to the presynaptic release site. The amount of transmitter released is a limiting factor in the size of a synaptic response. The currents that I recorded, on the other hand, were elicited in response to externally applied glutamate, and therefore could be made larger or smaller simply by adjusting the amplitude of

iontophoretic current. This cannot be representative of the “strength” of the postsynaptic region I am affecting.

Since the time course of glutamate clearance is unaffected by the amount of uncaged glutamate<sup>20</sup>, releasing more glutamate by increasing the amplitude of iontophoretic current would not substantially increase the amount of dendritic surface area affected. However, it would increase the higher concentration of glutamate within the affected dendritic area. This could cause a larger evoked current by binding postsynaptic receptors more frequently, while also recruiting a few areas farther away from the site of iontophoresis. This is represented schematically in **Figure 11(c)**. When the receptors saturate, the evoked response will not increase even if the iontophoretic current is increased. A larger response, then, could be evoked only by increasing the duration of the iontophoretic current.

There could be a few reasons why a larger iontophoresis evoked current appeared to correspond to a preference for LTD over LTP (**Figure 9(a)**). The first is similar to the idea presented in **Figure 11(a)**. However, this analysis was done for the time of peak of the evoked glutamate response as a whole. All postsynaptic NMDA receptors would be depolarized at the same time, but glutamate would not be available at all sites at the same time. Glutamate would reach closer receptors sooner than farther ones; if larger AMPA responses can be assumed to indicate that more glutamate was being bound by postsynaptic receptors, then there would be more NMDA receptors that bind glutamate later. The negative timing experienced by later receptors could encourage induction of LTD over LTP.

Iontophoretically evoked responses are representative of both synaptic and extrasynaptic receptors. The composition of an NMDA receptor is a key arbiter of its activation kinetics: current responses of NR2B-subunit containing receptors peak later, and last longer, compared to

NR2A-subunit containing receptors. For ages P14 to P20, it is not clear if assembly of NR2A subunits at synaptic sites is as complete as it is in older adult animals (See **Introduction**), but the relative fraction of NMDA current mediated by NR2A-subunit containing receptors are higher at synapses, and that mediated by NR2B-subunit, higher extrasynaptically. Therefore, if iontophoresis evokes more responses from extrasynaptic sites than from synaptic sites, for the same value of  $\Delta t$ , the influx of  $\text{Ca}^{++}$  would be slower in the former than in the latter. This would encourage LTD over LTP for larger evoked currents.

Spines are fairly evenly spaced along the dendrite, so it is not clear why an increase in glutamate spread laterally, along the dendritic surface, would recruit a greater proportion of extrasynaptic receptors than synaptic receptors. However, since spines protrude from the dendritic surface 0.5 to 1  $\mu\text{m}$  in height, synaptic receptors seated on the spine head are more likely to be saturated with glutamate, during small evoked currents, than extrasynaptic receptors that lie between the spines. Larger evoked currents could spread to more extrasynaptic sites by diffusing past the spines. Alternatively, an increase in evoked currents could indicate an equal proportion of increase in the numbers of extrasynaptic and synaptic NMDA receptors activated, but differences in sensitivity, saturation levels and signaling thresholds of the two NMDA receptor types could cause extrasynaptic NMDA receptors to have a greater influence on the plasticity outcome, resulting in LTD.

There also seems to be an age dependent preference for LTD over LTP (**Figure 9(c)**). While it is not unexpected that younger animals would tend to show LTD (see **Introduction**), this result was surprising, since all the animals I used were within their third week of postnatal development. Important transitions occur during this time, including preferential expression of extrasynaptic NR2B-containing receptors, synaptic expression of NR2A-containing receptors,

and gradual increase in the rate of glutamate uptake. Younger age would, therefore, imply a bias towards NR2B activation by evoked glutamate, and subsequent induction of LTD. It is possible that dendritic factors change quickly, from day to day of growth, during this week, resulting in the correlation seen in **Figure 9(c)**. That the correlation of plasticity outcome to age was not significant may be due to slightly different growth rates in different animals skewing the small sample size.

### 4.3 TECHNICAL OBSERVATIONS

The fundamental goal of this project was to establish, evaluate and refine the technique of microiontophoresis for the study of spike timing dependent plasticity in hippocampal slices. The experimental results revealed important issues that can be improved in future endeavors.

Although onset latency was measured in these experiments under the assumption that it would capture changes due to movement of the tip of the iontophoresis electrode, the data revealed that it was not reliable as a monitor of tip stability, except in the case of very large or sudden tip movement. If closer sites were sensitizing or desensitizing, this would be indistinguishable from a movement in the pipette location. Moreover, in LTD experiments, as the currents depressed and signal to noise ratio rose, it was not possible to get a reliable time of current onset. One could reject such experiments because of the difficulty in monitoring onset latency. If it were possible to monitor tip stability visually, and conduct long term experiments demonstrating invariance of tip position, this would be better evidence of the fact that the tip of the iontophoresis electrode is stable.

Due to the natural variability in baseline evoked response (as seen in **Figure 2**), a long initial period of test pulses (at least 10-15 minutes) would be necessary to prove that the initial evoked responses were not increasing or decreasing independent of induction protocol. Since the goal of these experiments were to uncover conditions that potentiate or depress iontophoretic applications of glutamate, it was important to avoid washout of factors required for LTP by waiting too long after whole cell configuration was achieved<sup>81</sup>. Therefore, I only collected an initial baseline of 5 minutes before applying the D-I protocol. One experiment showed successful induction of LTP even when induction protocol was applied 1 hour after the beginning of whole cell clamp, so for future experiments, it may be safe to extend the initial baseline to 10 or 15 minutes before D-I protocol is applied.

In planning experiments on STDP, it would be important to establish a priori limits on initial conditions more strictly than I had initially thought. The age of animals would best be limited to a range of two or three days, perhaps, and evoked glutamate current size limited to 50-60 pA, for homogenous experimental conditions.

In all of my experiments, I have used voltage clamp, instead of the more popular choice of current clamp, during induction protocols. Since I have established that it is possible to induce LTP and LTD by depolarizing in voltage clamp, without letting the neuron spike freely, future experiments can be done for parametric evaluation of dependence of plasticity on duration or magnitude of depolarization. Since my methods induced and expressed plasticity without requiring presynaptic transmitter release, an exceptionally useful application of iontophoretic STDP would be investigation using  $\text{Ca}^{++}$  channel blockers.

Since only AMPA receptors were recording during the experiments, I have to estimate how activation times affect the NMDA current based on AMPA current recordings. An

interesting experiment would be to use glutamate and NMDA in adjoining barrels of a multibarreled iontophoresis pipette. Glutamate could be used to elicit test pulses, but NMDA used during the induction protocol. The observed potentiation/depression of the glutamate evoked response could then be more accurately compared to NMDA receptor dependent differences.

## 5.0 TABLES

**Table 1.** Kinetics of  $I_{\text{AMPA}}$  and  $I_{\text{NMDA}}$

Values expressed as mean  $\pm$  standard error of 12 recorded currents ( $n = 1$ )

	Peak amplitude (pA)	Onset latency (ms)	Time to Peak (ms)	Half-width of current (ms)	20%-80% Rise Time (ms)	80%-20% Decay Time (ms)
$I_{\text{AMPA}}$ , in response to $I_{\text{iont}} = -100$ nA for 0.5 ms	$40.1 \pm 1.4$	$2.9 \pm 0.2$	$10.7 \pm 0.3$	$14.1 \pm 0.5$	$4.2 \pm 0.3$	$12.5 \pm 0.6$
$I_{\text{NMDA}}$ , in response to $I_{\text{iont}} = -100$ nA for 1 ms	$12.6 \pm 2.0$	$3.5 \pm 0.3$	$25.8 \pm 1.9$	$23.3 \pm 2.7$	$15.7 \pm 1.7$	$29.3 \pm 3.8$
$I_{\text{NMDA}}$ , in response to $I_{\text{iont}} = -200$ nA for 1 ms	$30.8 \pm 0.9$	$3.5 \pm 0.2$	$29.9 \pm 1.0$	$40.3 \pm 1.6$	$16.5 \pm 1.2$	$41.8 \pm 2.4$
$I_{\text{NMDA}}$ , in response to $I_{\text{iont}} = -250$ nA for 1 ms	$39.6 \pm 1.2$	$4.6 \pm 0.2$	$28.6 \pm 0.5$	$42.4 \pm 1.8$	$15.4 \pm 1.0$	$46.9 \pm 2.0$

**Table 2.**  $I_{\text{AMPA}}$  for different amplitudes of iontophoretic current

Values are expressed as measurements taken from single recorded currents ( $n = 1$ )

$I_{\text{AMPA}}$ In response to 0.1 ms of glutamate iontophoresis	Peak amplitude (pA)	Onset latency (ms)	Time to Peak (ms)	Half-width of current (ms)	20%-80% Rise Time (ms)	80%-20% Decay Time (ms)
$I_{\text{iont}} = -80$ nA	72.1	0.3	4.5	10.5	2.5	11.2
$I_{\text{iont}} = -100$ nA	111.5	0.3	4.8	9.5	2.4	9.9
$I_{\text{iont}} = -200$ nA	251.9	0.4	6	11.0	2.4	11.1
$I_{\text{iont}} = -300$ nA	289.1	0.3	6.5	12.0	2.4	10.2
$I_{\text{iont}} = -400$ nA	282.6	0.3	6.1	11.6	2.0	9.1
$I_{\text{iont}} = -500$ nA	324.3	0.2	6.2	12.0	2.0	9.6

## 6.0 FIGURES

Figure 1

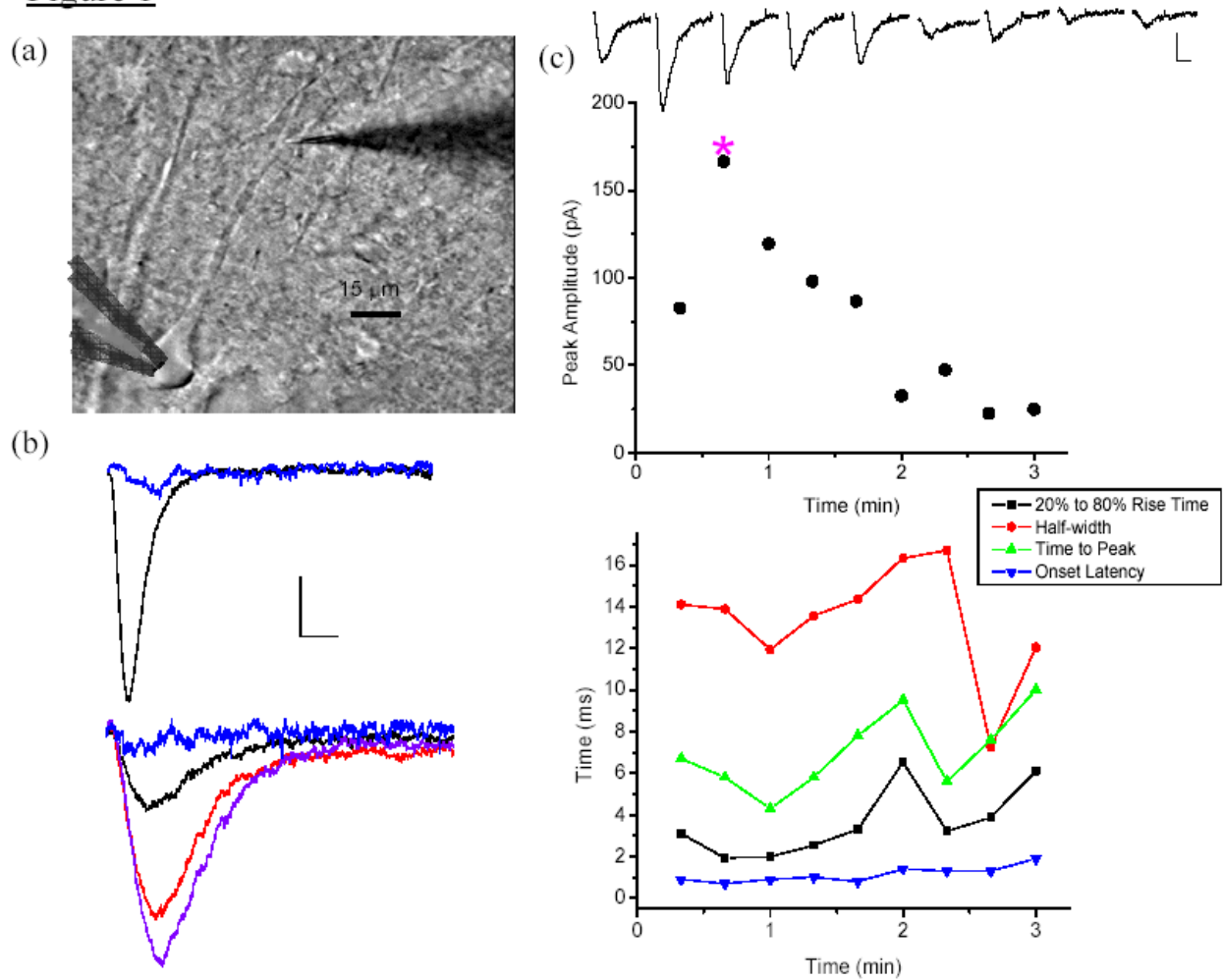


**Figure 1: Characterization of the current evoked by glutamate microiontophoresis.**

(a) Image of a pyramidal neuron with the iontophoresis electrode on the apical dendrite 60  $\mu\text{m}$  away from the soma, recording electrode at the soma. (Scale bar: 15  $\mu\text{m}$ )

- (b) Examples of glutamate evoked responses recorded at the soma of a pyramidal neuron held at  $V_m = -70$  mV; iontophoresis on dendrite at 50  $\mu\text{m}$ . The responses shown are averages of 12 responses, elicited and recorded at the rate of 6 per minute, with TTX (1  $\mu\text{M}$ ) in all extracellular solutions to inhibit polysynaptic activation. Data shown are from a single neuron. *Left*: Regular ACSF with TTX was used as the bath solution; iontophoresis of -100 nA for 0.5 ms (*black*); current abolished when NBQX (10  $\mu\text{M}$ ) was added (*blue*). *Right*: ACSF with 0  $\text{Mg}^{++}$  + NBQX.; iontophoresis of -100 nA for 1 ms (*black*), then -200 nA (*red*), and -250 nA (*purple*); current abolished when APV (50  $\mu\text{M}$ ) was added (*blue*). Calibration: 40 pA, 10 ms.
- (c) Example of the effect of movement of the iontophoretic electrode towards and away from the dendrite. Data shown are from a single neuron. *Inset*: Evoked currents; Calibration: 40 pA, 10 ms. *Top*: Peak amplitude of evoked current plotted against time. Iontophoresis electrode is in a different position at every recorded point. Asterisk (\*) marks point closest to the dendrite, after which data were recorded as the iontophoresis electrode was being withdrawn, away from the dendrite, in very small increments. *Bottom*: Other characteristics of the evoked current as they change with movement.

**Figure 2**

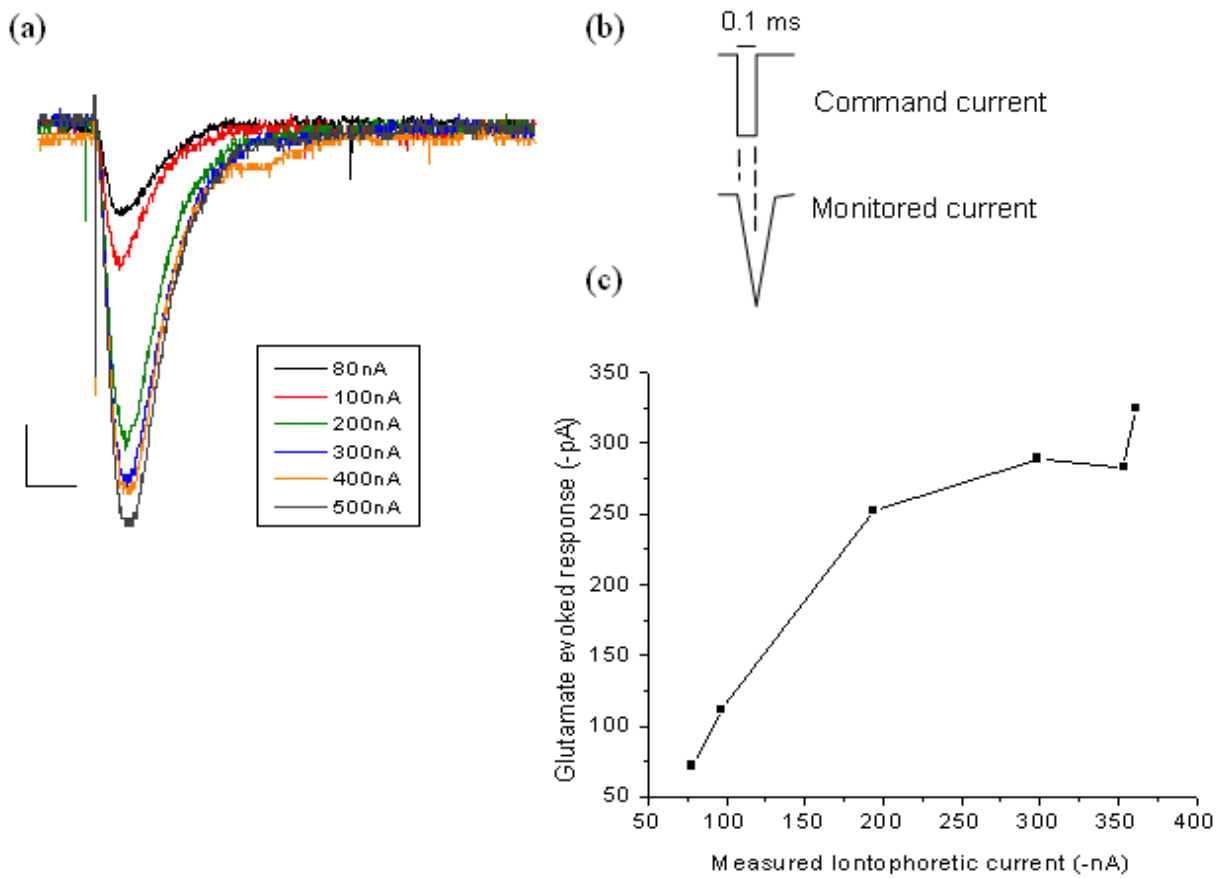


**Figure 2: Fidelity of iontophoretic stimulus**

- (a) Examples of increase in AMPA current response, recorded at the soma of a neuron held at  $V_m = -59$  mV in regular ACSF with TTX; amplitude of the iontophoretic current was progressively increased. Legend shows amplitude of iontophoretic current applied, for 0.1 ms each. Data shown are from a single neuron. Calibration: 50 pA, 10 ms.
- (b) Schematic representation of the discrepancy between command current and monitored current.
- (c) Relationship of glutamate evoked response to iontophoretic current (as measured through the current monitor).

**Figure 3**

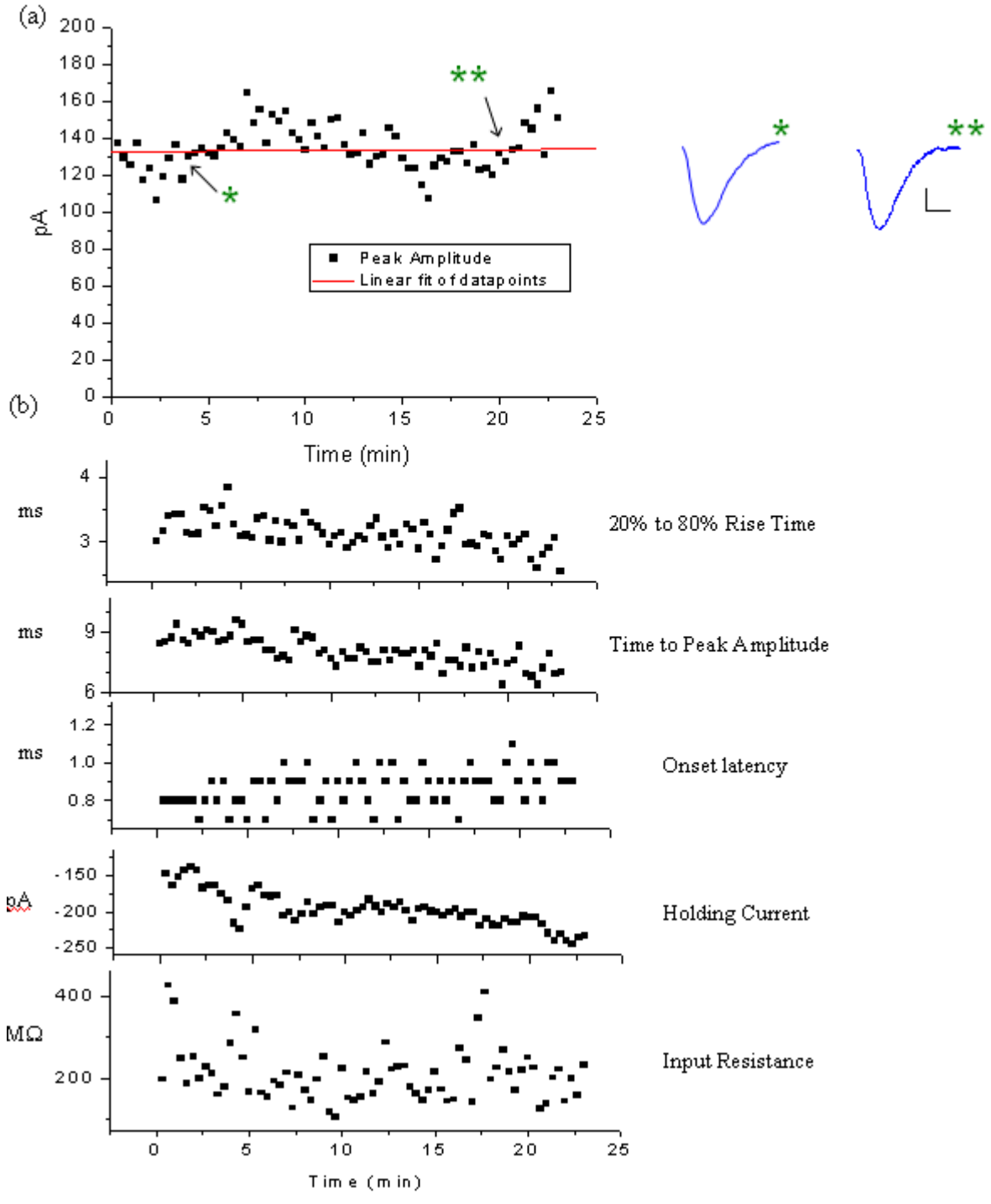


**Figure 3: Reliability of glutamate evoked current over time**

Responses were recorded with TTX (1  $\mu$ M) in the extracellular ACSF solution; glutamate iontophoresis on dendrite at 100  $\mu$ m. Responses were elicited and recorded at the rate of 3 per minute. Data shown are from a single neuron.  $I_{\text{iont}} = -200$  nA, for 0.1 ms.

(a) Peak amplitude varies over time, but a linear fit (slope = 0.06) over 23 minutes shows no net rundown or sensitization of the evoked response over time. *Right:* Sample evoked currents at time 4 minutes (single asterisk) and 21 minutes (double asterisk). Calibration: 40 pA, 10 ms.

(b) Indicated parameters measured from the cell used for (a) are plotted as a function of time.

**Figure 4**

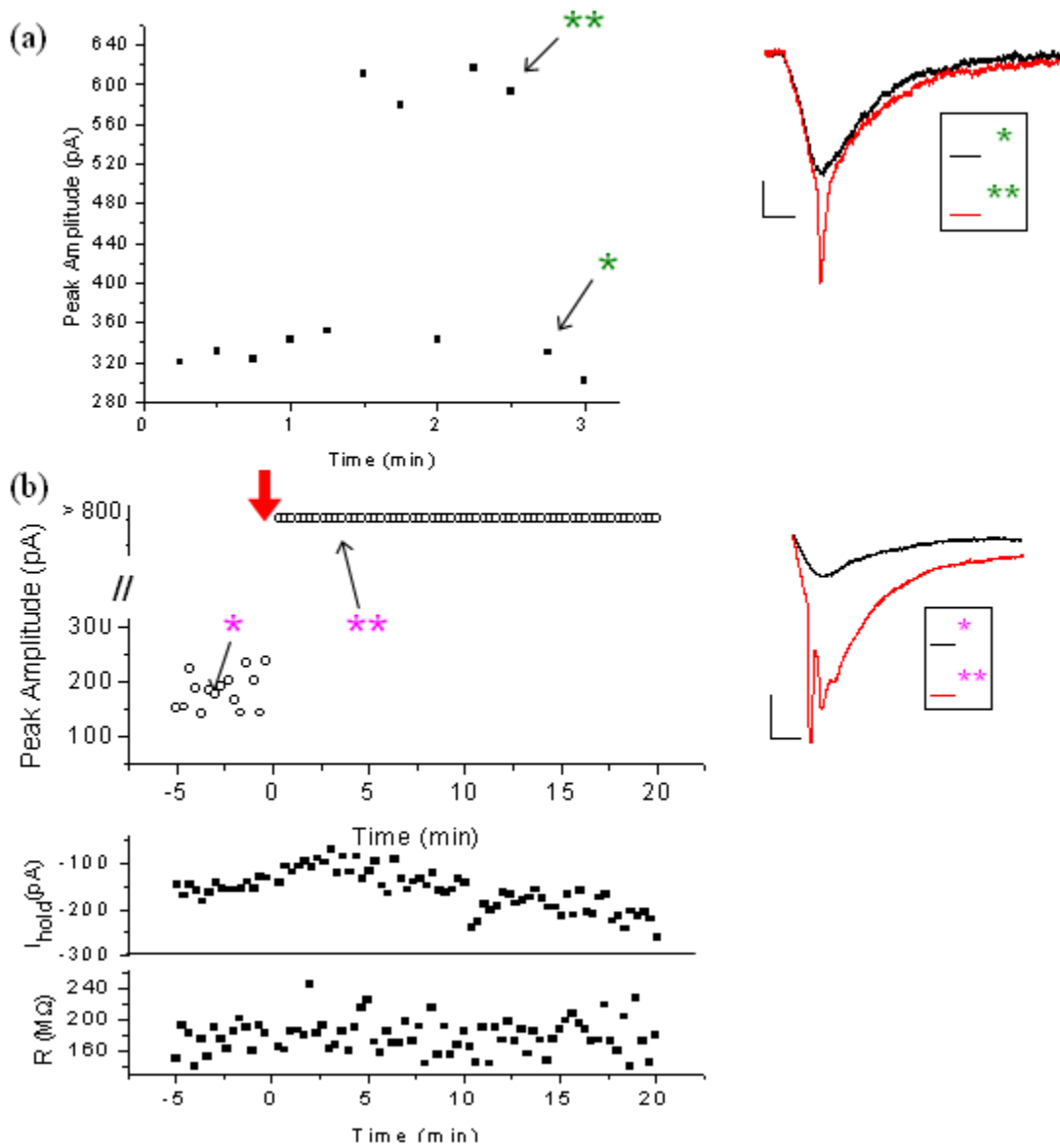


**Figure 4: Glutamate iontophoresis activates fast sodium currents despite voltage clamp**

Responses were recorded in regular ACSF solution; glutamate iontophoresis on dendrite at 100  $\mu\text{m}$ . Each point shows one response; responses were recorded at the rate of 3 per minute.

(a) *Left*: Iontophoretic current of -100 nA was applied for 3 ms, once every 20 seconds, for 3 minutes. While most of the evoked currents had a peak amplitude between 320 and 360 pA, a few had drastically larger ( $\sim 600$  pA) amplitudes. *Right*: Sample currents

corresponding to datapoints marked in the plot on left. While the smaller current (*single asterisk, black line*) looks like an AMPA current, the larger amplitude current (*double asterisk, red line*) exhibits a fast rising component (“spike”) that could be due to voltage activated Na<sup>+</sup> channels on dendritic membrane that is not fully clamped to -59 mV by the voltage clamp at the soma. Data shown are from a single neuron. Such spikes did not appear when TTX (1 μM) was used in the extracellular recording solution (not shown). Calibration: 100 pA, 20 ms.

(b) *Left*: Iontophoretic current of -300 nA was applied for 0.2 ms, once every 20 seconds, for 5 minutes, taking care that the evoked current was not activating fast Na<sup>+</sup> currents. After 5 minutes, a positive (+10ms) pairing protocol was applied (*solid red arrow*). Iontophoresis was then resumed at the rate of once per 20 seconds, for 20 minutes. All evoked currents in the latter 20 minutes exhibited spikes of amplitude >800 pA. Data shown are from a single neuron. *Right*: Sample currents corresponding to datapoints. Calibration: 200 pA, 20 ms.

**Figure 5**

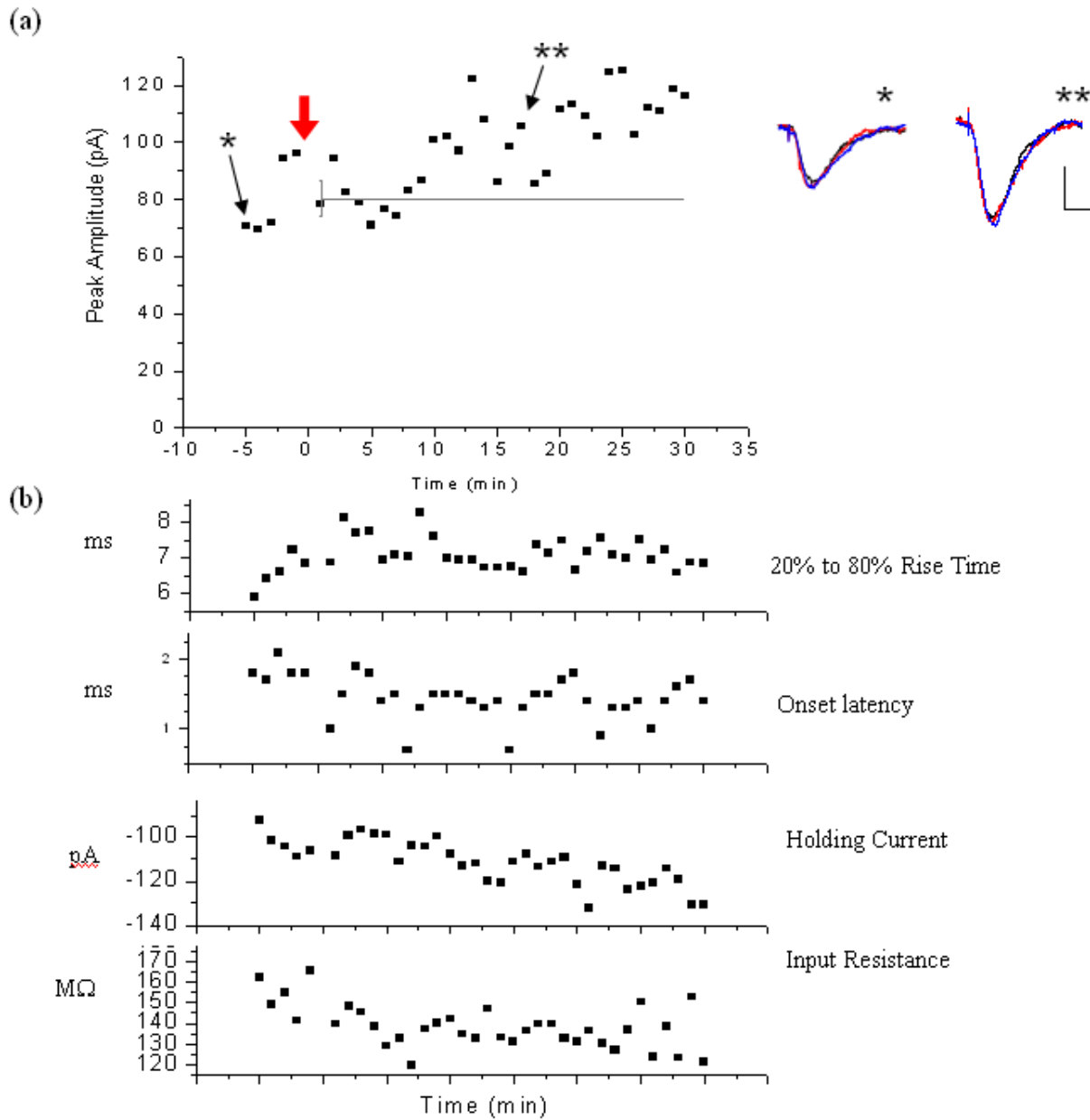


**Figure 5: Positive pairing induction protocol can lead to potentiation of glutamate evoked response (n = 5 out of 9)**

Responses were recorded with TTX (1  $\mu$ M) in the extracellular ACSF solution; glutamate iontophoresis on dendrite at 100  $\mu$ m. Each point is average of three sequential responses over the

course of 1 minute; responses were elicited and recorded at the rate of 3 per minute. Data shown are from a single neuron.  $I_{\text{iont}} = -400 \text{ nA}$ , for 0.2 ms.

(a) Positive D-I protocol was applied (*solid red arrow*) after 5 minutes of test pulses. The peak amplitude averaged over time between 15 and 20 minutes after D-I protocol ( $95.89 \pm 4.45 \text{ pA}$ ) was 19.3% greater than the average peak amplitude during the initial 5 minute baseline ( $80.38 \pm 6.1 \text{ pA}$ ). *Inset*: Examples of three sequential currents that were averaged for measurements plotted at -5 minutes (single asterisk) and 17 minutes (double asterisk). Calibration: 50 pA, 20 ms.

(b) Indicated parameters measured from the cell used for (a) are plotted as a function of time.

**Figure 6**

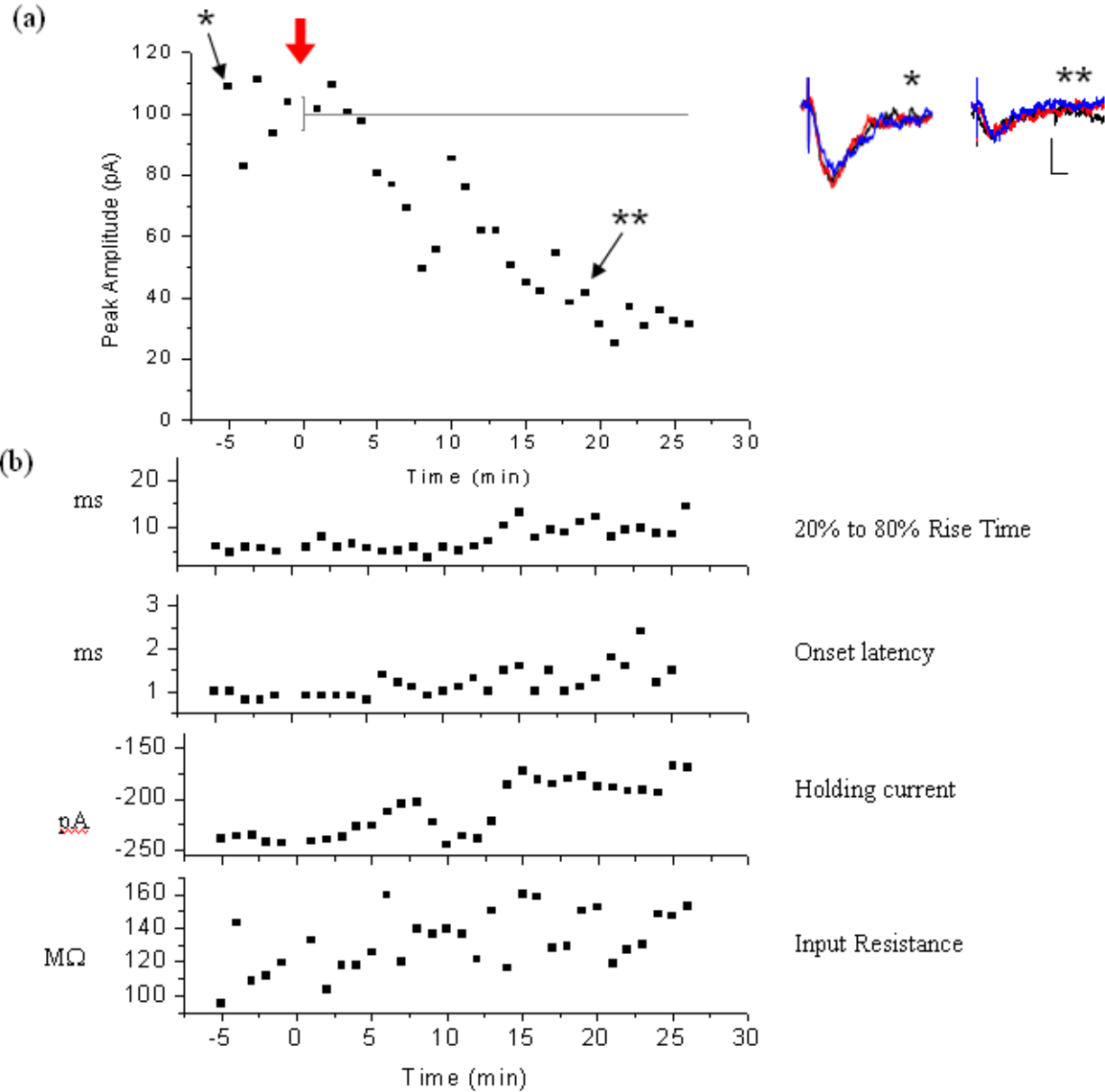


**Figure 6: Positive pairing induction protocol can lead to depression of glutamate evoked response (n = 4 out of 9)**

Responses were recorded with TTX (1  $\mu$ M) in the extracellular ACSF solution; glutamate iontophoresis on dendrite at 100  $\mu$ m. Each point is average of three sequential responses over

the course of 1 minute; responses were elicited and recorded at the rate of 3 per minute. Data shown are from a single neuron.  $I_{\text{iont}} = -150 \text{ nA}$ , for 0.3 ms.

(a) Positive D-I protocol was applied (*solid red arrow*) after 5 minutes of test pulses. The peak amplitude averaged over time between 15 and 20 minutes after D-I protocol ( $42.14 \pm 3.09 \text{ pA}$ ) was 57.9% decreased from the average peak amplitude during the initial 5 minute baseline ( $100.08 \pm 5.21 \text{ pA}$ ). *Inset*: Examples of three sequential currents that were averaged for measurements plotted at -5 minutes (single asterisk) and 19 minutes (double asterisk). Calibration: 50 pA, 20 ms.

(b) Indicated parameters measured from the cell used for (a) are plotted as a function of time.

**Figure 7**

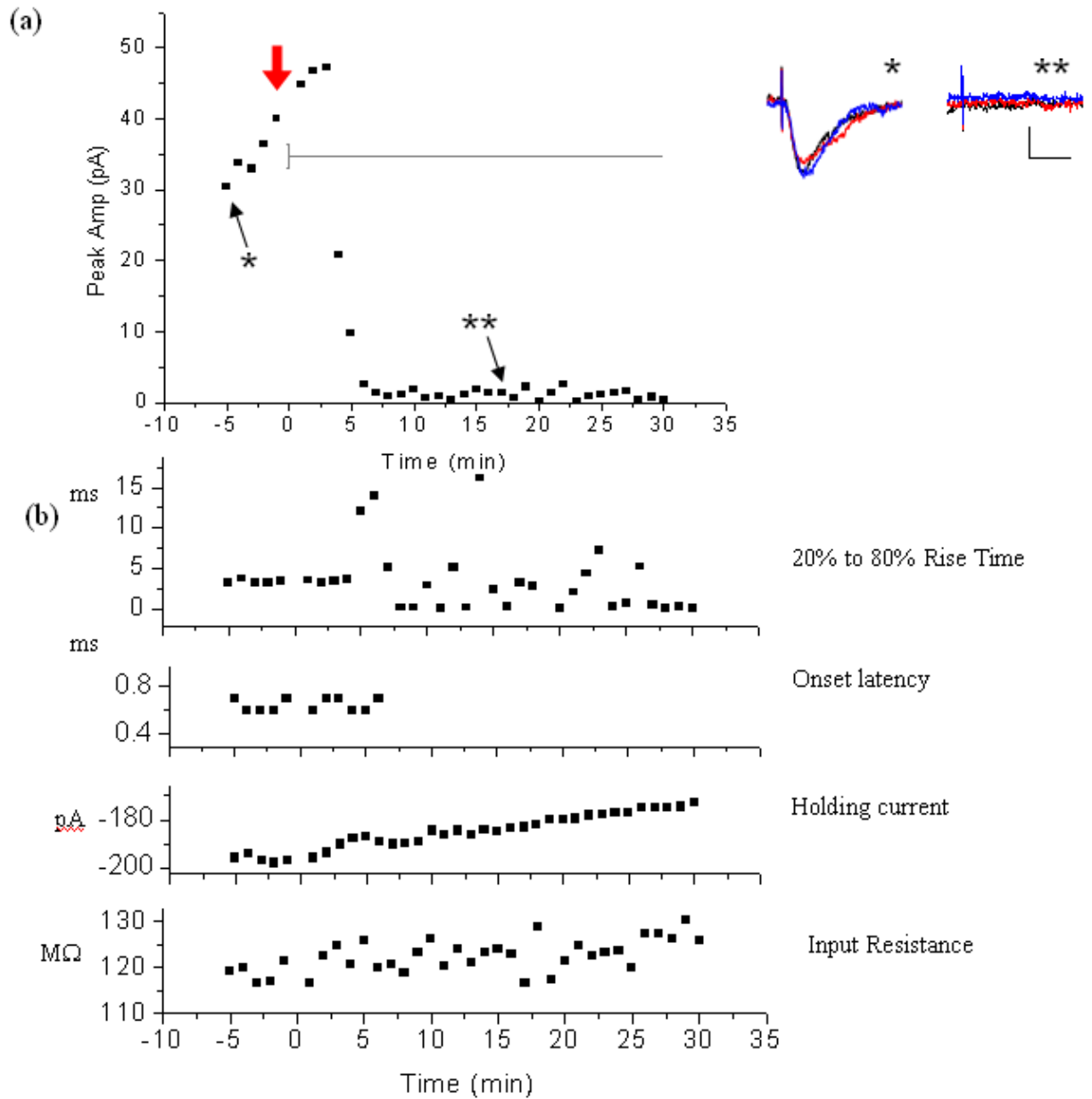


**Figure 7: Negative pairing induction protocol leads to depression of glutamate evoked response (n = 4 out of 4)**

Responses were recorded with TTX (1  $\mu$ M) in the extracellular ACSF solution; glutamate iontophoresis on dendrite at 100  $\mu$ m. Each point is average of six sequential responses over the

course of 1 minute; responses were elicited and recorded at the rate of 6 per minute. Data shown are from a single neuron.  $I_{\text{iont}} = -70$  nA, for 0.1 ms.

(a) Negative D-I protocol was applied (*solid red arrow*) after 5 minutes of test pulses. The peak amplitude averaged over time between 15 and 20 minutes after D-I protocol ( $1.21 \pm 0.31$  pA) was 96.5% decreased from the average peak amplitude during the initial 5 minute baseline ( $34.72 \pm 1.64$  pA). *Inset*: Examples of three sequential currents that were averaged for measurements plotted at -5 minutes (single asterisk) and 18 minutes (double asterisk). Calibration: 20 pA, 20 ms.

(b) Indicated parameters measured from the cell used for (a) are plotted as a function of time.

**Figure 8**

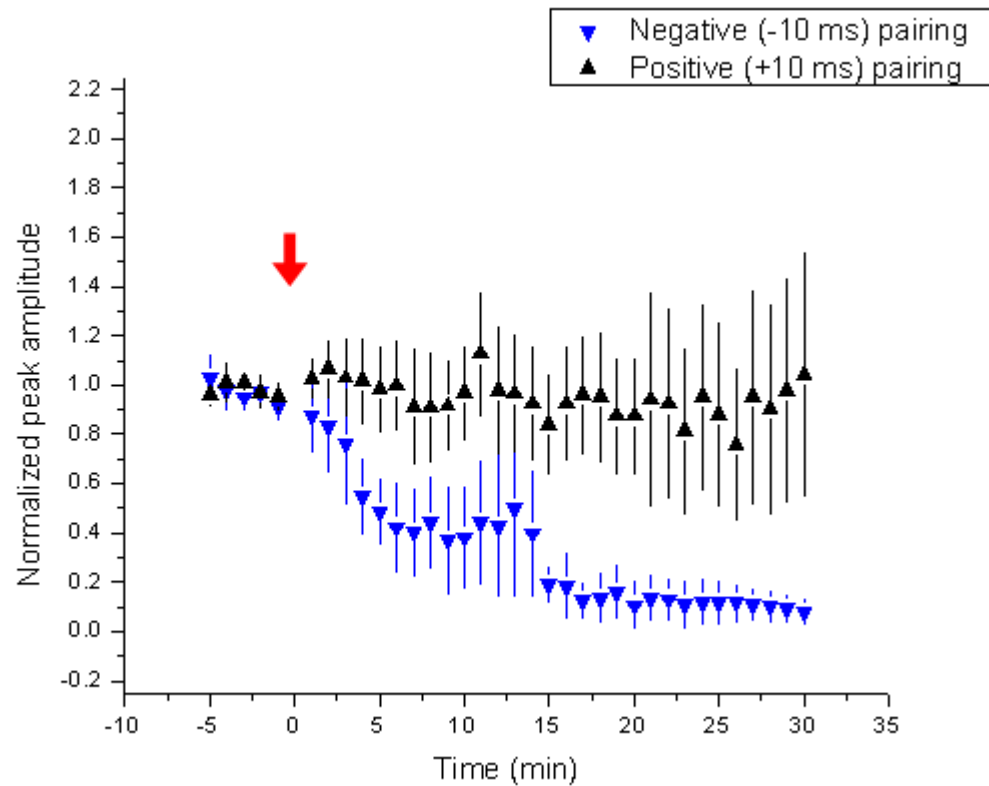


**Figure 8: Induction protocol is an important determinant of STDP outcome**

Summary of all experiments, positive (n = 9, *black triangles*,  $-8.2 \pm 23.0\%$ ) and negative (n = 4, *blue triangles*,  $-85.7 \pm 7.7\%$ ) pairing protocol. Data points represent mean  $\pm$  S.E.M. per minute.

While the negative pairing protocol induces LTD, the positive pairing protocol produces no net change from initial baseline period. Outcomes of positive and negative pairings are not significantly different ( $p > 0.05$ , t-test).

**Figure 9**

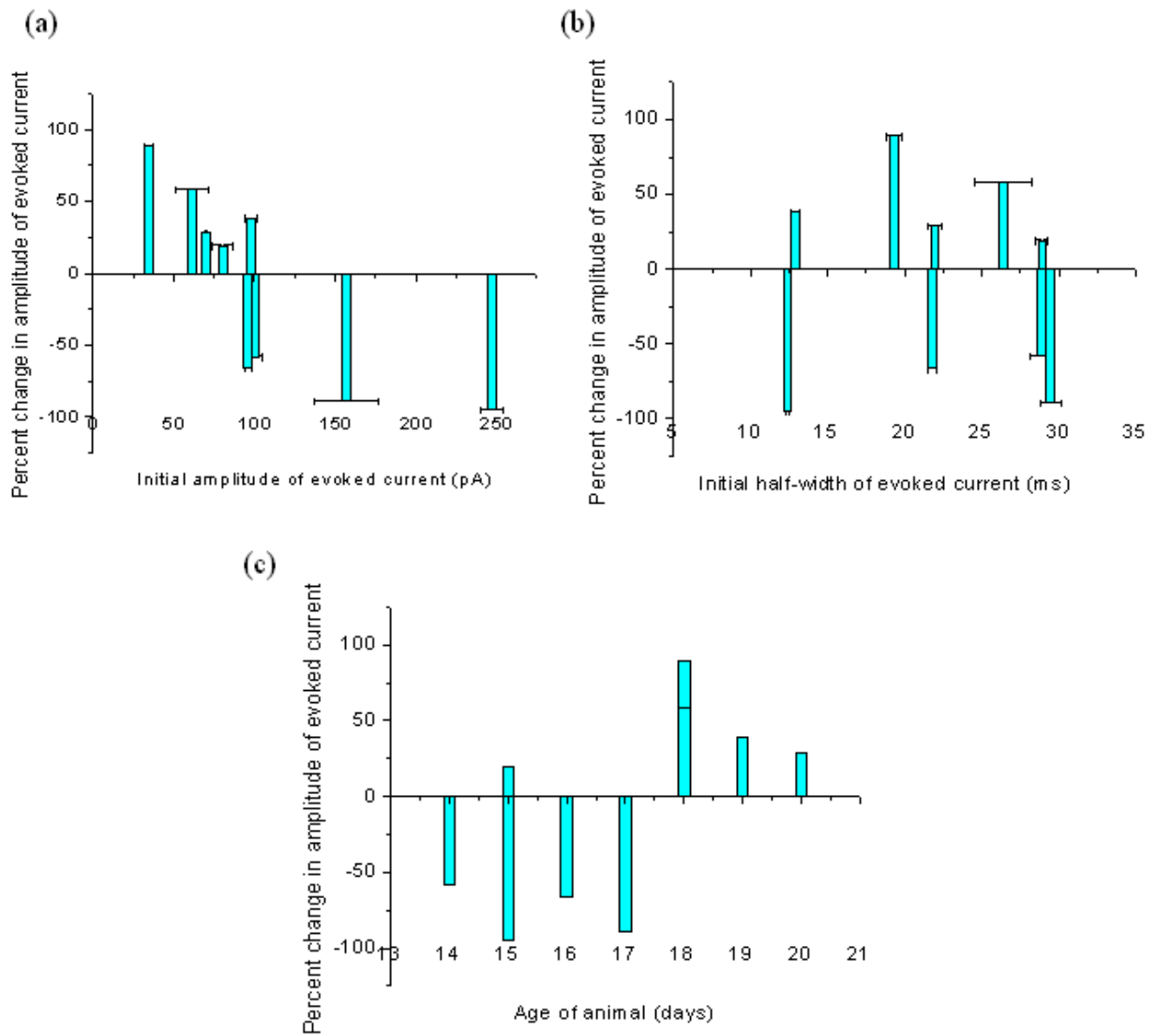


**Figure 9: Initial conditions influence induction of LTP in response to positive pairing of glutamate iontophoresis and depolarization**

(a) Percent change in glutamate evoked current plotted as a function of average initial peak amplitude,  $n = 9$ . The initial amplitude correlates strongly with negative percent change ( $r = -0.80$ ,  $p = 0.01$ ).

(b) Percent change in glutamate evoked current plotted as a function of average initial half-width,  $n = 9$ . The initial half-width does not show a correlation to percent change in current ( $r = -0.08$ ,  $p = 0.83$ ).

(c) Percent change in glutamate evoked current plotted as a function of age of the animal,  $n = 9$ . There appears to be a switch from decrease in amplitude to increase in amplitude as the age of the animal increases, but the correlation is not significant ( $r = 0.62$ ,  $p = 0.07$ ).

**Figure 10**

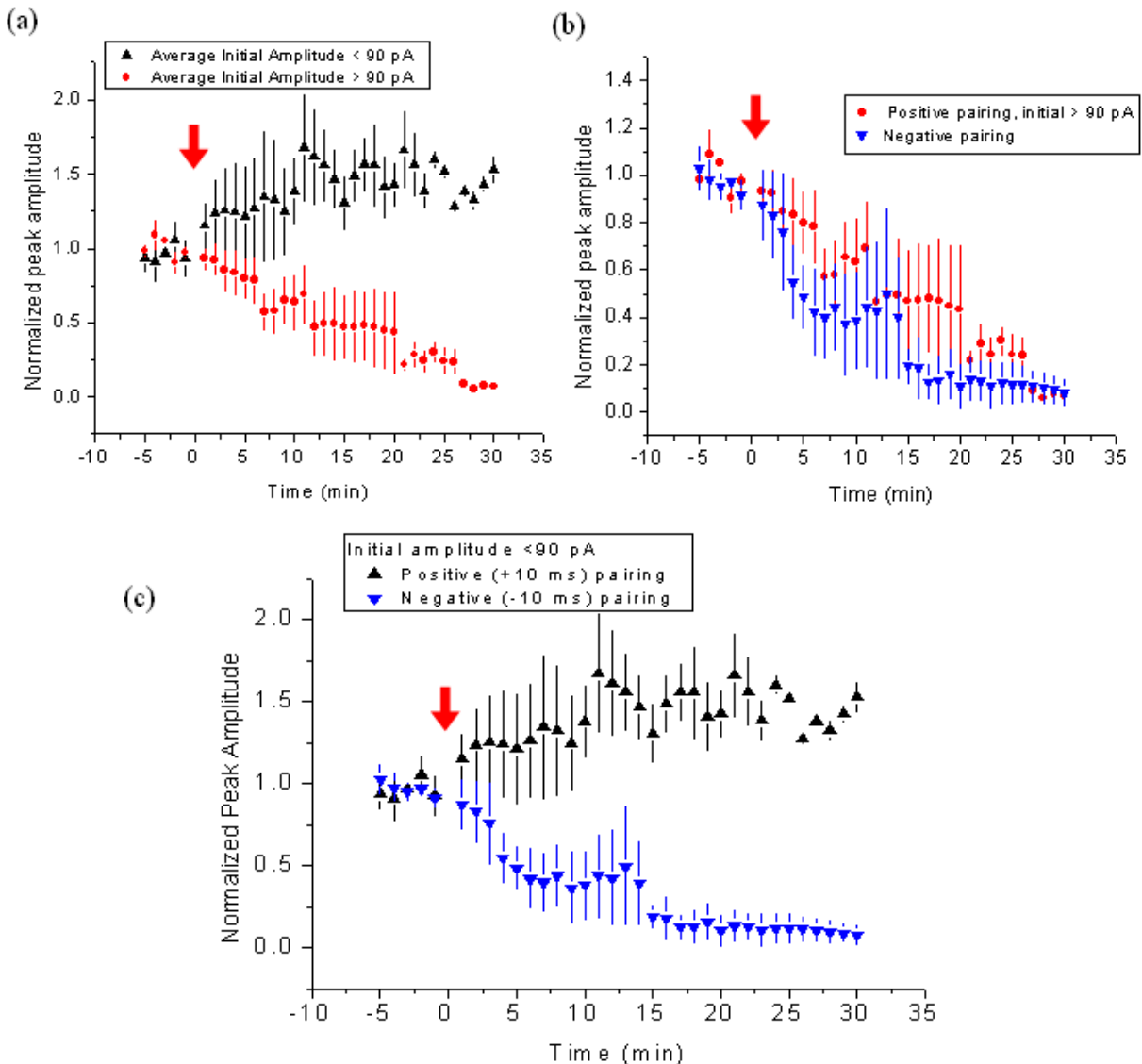


**Figure 10:** When initial currents are  $< 90$  pA in amplitude, positive D-I pairing results in LTP, while negative D-I pairing results in LTD

(a) Positive pairing experiments are grouped into: initial amplitude  $< 90$  pA (*black*):  $n = 4$ , mean percent change was  $48.9 \pm 15.8$ ; initial amplitude  $> 90$  pA (*red*):  $n = 5$ , mean percent change was  $-53.8 \pm 24.1$ ; difference between the two groups is significant ( $p < 0.05$ , t-test)

- (b) When overlaid, the depression following negative pairing (*blue*, same as in **Figure 8**), and the depression following positive pairing in currents with initial amplitude  $> 90$  pA (*red*, same as in (a)), show the same trend over time
- (c) When only currents with initial amplitude  $< 90$  pA are considered, positive pairing induction leads to LTP (*black*, same as in (a)), negative pairing data (*blue*, same as in (b)) show LTD; difference between the two groups is significant ( $p < 0.01$ , t-test)

**Figure 11**

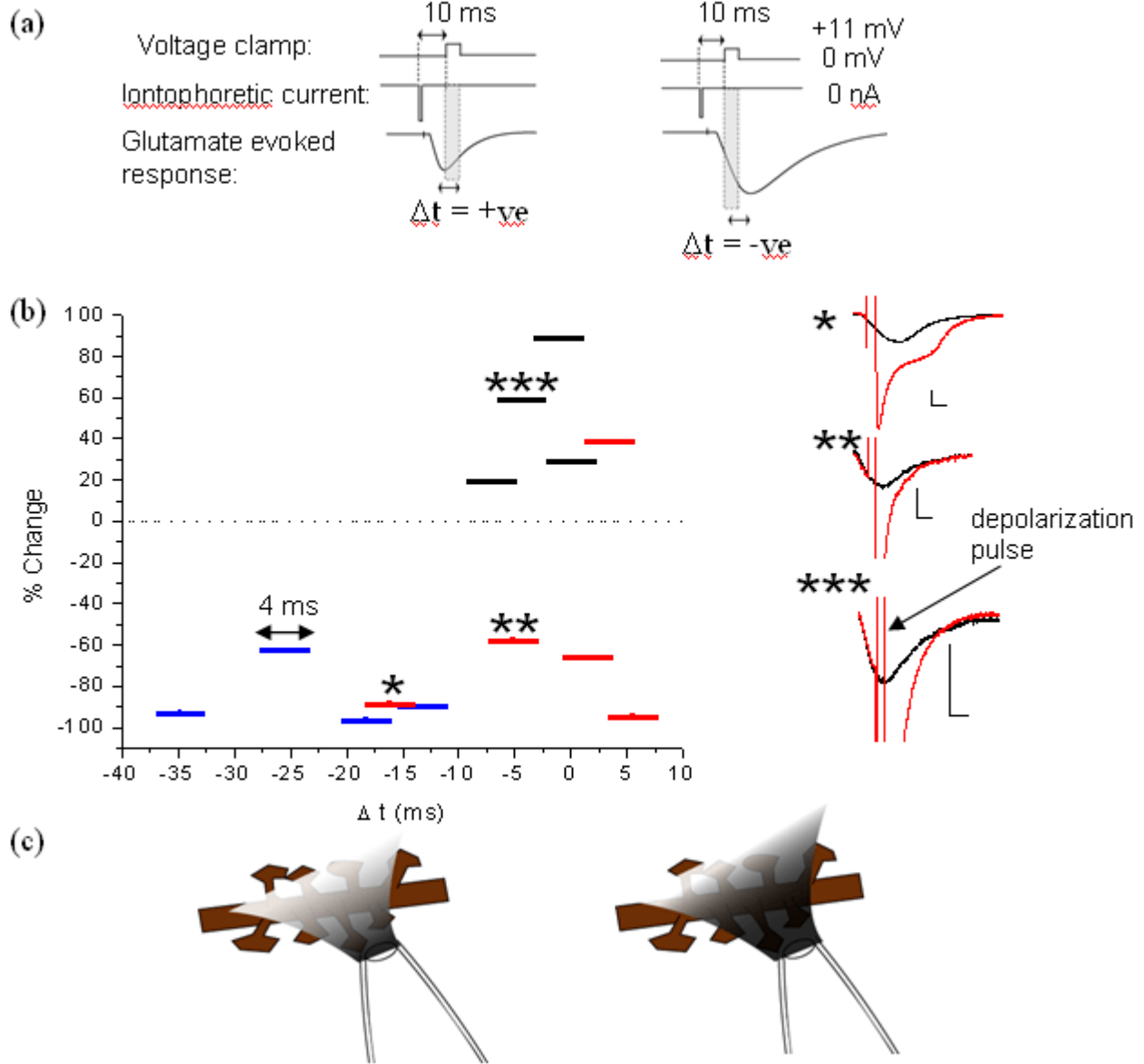


**Figure 11: Initial conditions influence induction of LTP in response to positive pairing of glutamate iontophoresis and depolarization**

(a) Schematic illustrating how the same +10 ms positive D-I protocol can result in a “negative” time interval ( $\Delta t$ ), i.e. depolarization occurs before peak glutamate response when the time it takes for the glutamate current to reach its peak is greater than 10 ms.

- (b) Results from all induction protocols, positive D-I with initial amplitude  $< 90$  pA (*black*), positive D-I with initial amplitude  $> 90$  pA (*red*), and negative D-I (*blue*), plotted as a function of  $\Delta t$ , where  $\Delta t$  is the time between the beginning of depolarization and the average (5 minutes) time to reach peak for initial baseline glutamate evoked currents. If depolarization arrived before evoked current reached its peak,  $\Delta t$  is negative. Width of each datapoint is 4 ms, corresponding to duration of depolarizing pulse. Initial amplitude of evoked currents does not correlate to  $\Delta t$  ( $r = 0.12$ ,  $p = 0.77$ ). (*Right*) Examples of relative timing of initial peak current (*black*) overlaid with the current when paired with depolarization (*red*) during the D-I protocol. Calibration: 100pA, 10 ms
- (c) Schematic representation of the spread of glutamate when iontophoresis onto a segment of dendrite evokes a glutamate response (*left*), and the spread of glutamate when the amplitude of iontophoretic current is increased to evoke a larger response (*right*). The darker shade indicates higher concentration of glutamate, reaching more spines and interspinal areas.

## BIBLIOGRAPHY

- 1 Andersen, P (1990) Synaptic integration in hippocampal CA1 pyramids. *Prog Brain Res* 83:215-22
- 2 Bagal AA, Kao JP, Tang CM, Thompson SM (2005) Long-term potentiation of exogenous glutamate responses at single dendritic spines. *Proc Natl Acad Sci U S A* 102(40): 14434-9
- 3 Bannister NJ, Larkman AU (1995) Dendritic morphology of CA1 pyramidal neurones from the rat hippocampus: II. Spine distributions. *J Comp Neurol* 360(1):161-71
- 4 Barria A, Malinow R (2005) NMDA receptor subunit composition controls synaptic plasticity by regulating binding to CaMKII. *Neuron* 48(2):289-301
- 5 Bayer KU, De Koninck P, Leonard AS, Hell JW, Schulman H (2001) Interaction with the NMDA receptor locks CaMKII in an active conformation. *Nature* 411(6839):801-5
- 6 Beattie EC, Carroll RC, Yu X, Morishita W, Yasuda H, von Zastrow M, Malenka RC (2000) Regulation of AMPA receptor endocytosis by a signaling mechanism shared with LTD. *Nat Neurosci* 3(12):1291-300

- 7 Berberich S, Punnakkal P, Jensen V, Pawlak V, Seeburg PH, Hvalby Ø, Köhr G (2005) Lack of NMDA receptor subtype selectivity for hippocampal long-term potentiation. *J Neurosci* 25(29):6907-10
- 8 Bi GQ, Poo MM (1998) Synaptic modifications in cultured hippocampal neurons: dependence on spike timing, synaptic strength, and postsynaptic cell type. *J Neurosci* 18(24):10464-72
- 9 Bi GQ, Poo MM (2001) Synaptic Modification by Correlated Activity: Hebb's Postulate Revisited. *Annu Rev Neurosci* (24):139-66
- 10 Bliss T, Schoepfer R (2004) Controlling the Ups and Downs of Synaptic Strength. *Science* 304(5673):973-74
- 11 Bliss TV, Lomo T (1973) Long-lasting potentiation of synaptic transmission in the dentate area of the anaesthetized rabbit following stimulation of the perforant path. *J Physiol* 232(2):331-56
- 12 Carnevale NT, Tsai KY, Claiborne BJ, Brown TH (1997) Comparative electrotonic analysis of three classes of rat hippocampal neurons. *J Neurophysiol* 78:703-20
- 13 Christie BR, Magee JC, Johnston D (1996) The role of dendritic action potentials and Ca<sup>2+</sup> influx in the induction of homosynaptic long-term depression in hippocampal CA1 pyramidal neurons. *Learn Mem* 3:160-9
- 14 Clements JD, Lester RA, Tong G, Jahr CE, Westbrook GL (1992) The time course of glutamate in the synaptic cleft. *Science* 258:1498-501

- 15 Cormier RJ, Mauk MD, Kelly PT (1993) Glutamate iontophoresis induces long-term potentiation in the absence of evoked presynaptic activity. *Neuron* 10(5):907-19
- 16 Crossman AR, Walker RJ, Woodruff GN (1974) Problems associated with iontophoretic studies in the caudate nucleus and substantia nigra. *Neuropharmacology* 13(6):547-552
- 17 Dan Y, Poo MM (2006) Spike timing-dependent plasticity: from synapse to perception. *Physiol Rev* 86(3):1033-48
- 18 Debanne D, Gähwiler BH, Thompson SM (1998) Long-term synaptic plasticity between pairs of individual CA3 pyramidal cells in rat hippocampal slice cultures. *J Physiol* 507(1):237-47
- 19 Diamond JS, Jahr CE (1997) Transporters buffer synaptically released glutamate on a submillisecond time scale. *J Neurosci* 17(12):4672-87
- 20 Diamond JS (2005) Deriving the glutamate clearance time course from transporter currents in CA1 hippocampal astrocytes: Transmitter uptake gets faster during development. *J Neurosci* 25(11):2906-16
- 21 Dong HW, Buonomano DV (2005) A technique for repeated recordings in cortical organotypic slices. *J Neurosci Methods* 146(1):69-75
- 22 Dudek SM, Bear MF (1992) Homosynaptic long-term depression in area CA1 of hippocampus and effects of N-methyl-D-aspartate receptor blockade. *Proc Natl Acad Sci U S A* 89:4363-7

- 23 Duguid I, Sjöström PJ (2006) Novel presynaptic mechanisms for coincidence detection in synaptic plasticity. *Curr Opin Neurobiol* 16(3):312-22
- 24 Eder M, Zieglängsberger W, Dodt HU (2002) Neocortical long-term potentiation and long-term depression: Site of expression investigated by infrared-guided laser stimulation. *J Neurosci* 22(17):7558-68
- 25 Flint AC, Maisch US, Weishaupt JH, Kriegstein AR, Monyer H (1997) NR2A subunit expression shortens NMDA receptor synaptic currents in developing neocortex. *J Neurosci* 17(7):2469-76
- 26 Froemke RC, Poo MM, Dan Y (2005) Spike-timing-dependent synaptic plasticity depends on dendritic location. *Nature* 434(7030):221-5
- 27 Gerkin RC, Lau PM, Nauen DW, Wang YT, Bi, GQ (2007) Modular Competition Driven by NMDA Receptor Subtypes in Spike-Timing-Dependent Plasticity. *J Neurophysiol* 97(4):2851-62
- 28 Golding NL, Mickus TJ, Katz Y, Kath WL, Spruston N (2005) Factors mediating powerful voltage attenuation along CA1 pyramidal neuron dendrites. *J Physiol* 568(1):69-82
- 29 Gustafsson B, Wigström H (1988) Physiological mechanisms underlying long-term potentiation. *Trends Neurosci* 11(4):156-62
- 30 Harris KM, Jensen FE, Tsao B (1992) Three-dimensional structure of dendritic spines and synapses in rat hippocampus (CA1) at postnatal day 15 and adult ages: implications

for the maturation of synaptic physiology and long-term potentiation. *J Neurosci* 12(7):2685-705

31 Häusser M, Spruston N, Stuart GJ (2000) Diversity and dynamics of dendritic signaling. *Science* 290(5492):739-44

32 Hayashi Y, Shi SH, Esteban JA, Piccini A, Poncer JC, Malinow R (2000) Driving AMPA receptors into synapses by LTP and CaMKII: Requirement for GluR1 and PDZ domain interaction. *Science* 287(5461):2262-7

33 Hebb, D (1949) *The Organization of Behavior*. New York: Wiley

34 Jack JJB, Noble D, Tsien RW (1975) *Electric Current Flow in Excitable Cells*. Oxford University Press

35 Johnson JW, Ascher P (1992) Equilibrium and kinetic study of glycine action on the N-methyl-D-aspartate receptor in cultured mouse brain neurons. *J Physiol* 455:339-65

36 Judkewitz B, Roth A, Häusser M (2006) Dendritic enlightenment: Using patterned two-photon uncaging to reveal the secrets of the brain's smallest dendrites. *Neuron* 50(2):180-3

37 Kampa BM, Letzkus JJ, Stuart GJ (2007) Dendritic mechanisms controlling spike-timing-dependent synaptic plasticity. *Trends Neurosci* 30(9):456-63

38 Kandler K, Katz LC, Kauer JA (1998) Focal photolysis of caged glutamate produces long-term depression of hippocampal glutamate receptors. *Nat Neurosci* 1(2):119-23

- 39 Koester HJ, Sakmann B (1998) Calcium dynamics in single spines during coincident pre- and postsynaptic activity depend on relative timing of back-propagating action potentials and subthreshold excitatory postsynaptic potentials. *Proc Natl Acad Sci U S A* 95(16):9596-601
- 40 Korkotian E, Oron D, Silberberg Y, Segal M (2004) Confocal microscopic imaging of fast UV-laser photolysis of caged compounds. *J Neurosci Methods* 133(1-2):153-9
- 41 Lalley, PM (1999) Ch 7: Microiontophoresis and Pressure Ejection, in: U. Windhorst, and H. Johansson (eds), *Modern Techniques in Neuroscience Research*. Springer Verlag
- 42 Liao D, Jones A, Malinow R (1992) Direct measurement of quantal changes underlying long-term potentiation in CA1 hippocampus. *Neuron* 9(6):1089-97
- 43 Liao D, Malinow R (1996) Deficiency in induction but not expression of LTP in hippocampal slices from young rats. *Learn Mem* 3(2-3):138-49
- 44 Liu L, Wong TP, Pozza MF, Lingenhoehl K, Wang Y, Sheng M, Auberson YP, Wang YT (2004) Role of NMDA receptor subtypes in governing the direction of hippocampal synaptic plasticity. *Science* 304(5673):1021-4
- 45 Lledo PM, Hjelmstad GO, Mukherji S, Soderling TR, Malenka RC, Nicoll RA (1995) Calcium/calmodulin-dependent kinase II and long-term potentiation enhance synaptic transmission by the same mechanism. *Proc Natl Acad Sci U S A* 92 (24):11175-9
- 46 Lynch MA (2004) Long-term potentiation and memory. *Physiol Rev* 84(1): 87-136

- 47 Magee JC, Johnston D (1997) A synaptically controlled, associative signal for Hebbian plasticity in hippocampal neurons. *Science* 275:209-13
- 48 Malenka RC, Bear MF (2004) LTP and LTD: an embarrassment of riches. *Neuron* 44(1): 5-21
- 49 Malenka RC, Nicoll RA (1999) Long-term potentiation--a decade of progress? *Science* 285:1870-4
- 50 Malgaroli A, Tsien RW (1992) Glutamate-induced long-term potentiation of the frequency of miniature synaptic currents in cultured hippocampal neurons. *Nature* 357(6374): 134-9
- 51 Markram H, Lübke J, Frotscher M, Roth A, Sakmann B (1997) Physiology and anatomy of synaptic connections between thick tufted pyramidal neurones in the developing rat neocortex. *J Physiol* 500 (2):409-40
- 52 Markram H, Lübke J, Frotscher M, Sakmann B (1997) Regulation of synaptic efficacy by coincidence of postsynaptic APs and EPSPs. *Science* 275(5297):213-5
- 53 Mason A, Nicoll A, Stratford K (2003) Synaptic transmission between individual pyramidal neurons of the rat visual cortex in vitro. *J Neurosci* 11(1): 72-84
- 54 Massey PV, Johnson BE, Moulton PR, Auberson YP, Brown MW, Molnar E, Collingridge GL, Bashir ZI (2004) Differential roles of NR2A and NR2B-containing NMDA receptors in cortical long-term potentiation and long-term depression. *J Neurosci* 24(36):7821-7828

- 55 Matsuzaki M, Ellis-Davies GC, Nemoto T, Miyashita Y, Iino M, Kasai H (2001) Dendritic spine geometry is critical for AMPA receptor expression in hippocampal CA1 pyramidal neurons. *Nat Neurosci* 4:1086-92
- 56 Matsuzaki M, Honkura N, Ellis-Davies GC, Kasai H (2004) Structural basis of long-term potentiation in single dendritic spines *Nature* 429, 761-766 (2004)
- 57 Mayer ML, Westbrook GL, Guthrie PB (1984) Voltage-dependent block by Mg<sup>++</sup> of NMDA responses in spinal cord neurones. *Nature* 309(5865):261-3
- 58 Momiyama A (2000) Distinct synaptic and extrasynaptic NMDA receptors identified in dorsal horn neurones of the adult rat spinal cord. *J Physiol* 523(3):621-8
- 59 Montgomery JM, Pavlidis P, Madison DV (2001) Pair recordings reveal all-silent synaptic connections and the postsynaptic expression of long-term potentiation. *Neuron* 29(3):691-701
- 60 Mulkey RM, Endo S, Shenolikar S, Malenka RC (1994) Involvement of a calcineurin/inhibitor-1 phosphatase cascade in hippocampal long-term depression. *Nature* 369(6480):486-8
- 61 Mulkey RM, Herron CE, Malenka RC (1993) An essential role for protein phosphatases in hippocampal long-term depression. *Science* 261:1051-5
- 62 Mulkey RM, Malenka RC (1992) Mechanisms underlying induction of homosynaptic long-term depression in area CA1 of the hippocampus. *Neuron* 9(5):967-75

- 63 Murnick JG, Dubé G, Krupa B, Liu G (2002) High-resolution iontophoresis for single-synapse stimulation. *J Neurosci Methods* 116(1):65-75
- 64 MVCS user manual, NPI Electronics
- 65 Nevian T, Sakmann B (2004) Single spine Ca<sup>2+</sup> signals evoked by coincident EPSPs and backpropagating action potentials in spiny stellate cells of layer 4 in the juvenile rat somatosensory barrel cortex. *J Neurosci* 24(7):1689-99
- 66 Nicoll RA, Malenka RC (1995) Contrasting properties of two forms of long-term potentiation in the hippocampus. *Nature* 377(6545):115-8
- 67 Nishiyama M, Hong K, Mikoshiba K, Poo MM, Kato K (2000) Calcium stores regulate the polarity and input specificity of synaptic modification. *Nature* 408(6812):584-8
- 68 O'Dell TJ, Kandel ER (1994) Low-frequency stimulation erases LTP through an NMDA receptor-mediated activation of protein phosphatases. *Learn Mem* 1(2):129-39
- 69 Petralia RS, Sans N, Wang YX, Wenthold RJ (2005) Ontogeny of postsynaptic density proteins at glutamatergic synapses. *Mol Cell Neurosci* 29(3):436-52
- 70 Pike FG, Meredith RM, Olding AW, Paulsen O (1999) Rapid report: Postsynaptic bursting is essential for "Hebbian" induction of associative long-term potentiation at excitatory synapses in rat hippocampus. *J Physiol* 518:571-6
- 71 Plant K, Pelkey KA, Bortolotto ZA, Morita D, Terashima A, McBain CJ, Collingridge GL, Isaac JT (2006) Transient incorporation of native GluR2-lacking AMPA receptors during hippocampal long-term potentiation. *Nat Neurosci* 9(5):602-4

- 72 Poncer JC, Esteban JA, Malinow R (2002) Multiple mechanisms for the potentiation of AMPA receptor-mediated transmission by alpha-Ca<sup>2+</sup>/calmodulin-dependent protein kinase II. *J Neurosci* 22(11):4406-11
- 73 Reyes A, Sakmann B (1999) Developmental switch in the short-term modification of unitary EPSPs evoked in layer 2/3 and layer 5 pyramidal neurons of rat neocortex. *J Neurosci* 19(10):3827-35
- 74 Rumbaugh G, Vicini S (1999) Distinct synaptic and extrasynaptic NMDA receptors in developing cerebellar granule neurons. *J Neurosci* 19(24):10603-10
- 75 Sabatini BL, Oertner TG, Svoboda K (2002) The life cycle of Ca<sup>2+</sup> ions in dendritic spines. *Neuron* 33(3):439-52
- 76 Sans N, Petralia RS, Wang YX, Blahos J 2nd, Hell JW, Wenthold RJ (2000) A developmental change in NMDA receptor-associated proteins at hippocampal synapses. *J Neurosci* 20:1260-71
- 77 Sjöström PJ, Häusser M (2006) A cooperative switch determines the sign of synaptic plasticity in distal dendrites of neocortical pyramidal neurons. *Neuron* 51(2):227-38
- 78 Sjöström PJ, Turrigiano GG, Nelson SB (2001) Rate, timing, and cooperativity jointly determine cortical synaptic plasticity. *Neuron* 32(6):1149-64
- 79 Spruston N, Schiller Y, Stuart G, Sakmann B (1995) Activity-dependent action potential invasion and calcium influx into hippocampal CA1 dendrites. *Science* 268(5208):297-300

- 80 Stanton PK, Winterer J, Zhang XL, Müller W (2005) Imaging LTP of presynaptic release of FM1-43 from the rapidly recycling vesicle pool of Schaffer collateral–CA1 synapses in rat hippocampal slices. *Eur J Neurosci* 22(10):2451-61
- 81 Stevens CF, Wang Y (1994) Changes in reliability of synaptic function as a mechanism for plasticity. *Nature* 371: 704–7
- 82 Stocca G, Vicini S (1998) Increased contribution of NR2A subunit to synaptic NMDA receptors in developing rat cortical neurons. *J Physiol* 507(1):13-24
- 83 Stone TW (1985) Microiontophoresis and Pressure Ejection. *IBRO Handbook Series: Methods in the Neurosciences, Vol.8*. Chichester: John Wiley & Sons
- 84 Stuart GJ, Sakmann B (1994) Active propagation of somatic action potentials into neocortical pyramidal cell dendrites. *Nature* 367(6458):69-72
- 85 Sweatt JD (1999) Toward a molecular explanation for long-term potentiation. *Learn Mem* 6:399-416
- 86 Tang YP, Shimizu E, Dube GR, Rampon C, Kerchner GA, Zhuo M, Liu G, Tsien JZ (1999) Genetic enhancement of learning and memory in mice. *Nature* 401(6748):63-9
- 87 Tovar KR, Westbrook GL (1999) The incorporation of NMDA receptors with a distinct subunit composition at nascent hippocampal synapses in vitro. *J Neurosci* 19(10): 4180-

- 88 Trommald M, Jensen V, Andersen P (1995) Analysis of dendritic spines in rat CA1 pyramidal cells intracellularly filled with a fluorescent dye. *J Comp Neurol* 353(2):260-74
- 89 Turner, DA (1984) Segmental cable evaluation of somatic transients in hippocampal neurons (CA1, CA3 and Dentate). *Biophys J* 46:73-84
- 90 Weitlauf C, Honse Y, Auberson YP, Mishina M, Lovinger DM, Winder DG (2005) Activation of NR2A-containing NMDA receptors is not obligatory for NMDA receptor-dependent long-term potentiation. *J Neurosci* 25(37):8386-90
- 91 Wenthold RJ, Prybylowski K, Standley S, Sans N, Petralia RS (2003) Trafficking of NMDA receptors. *Annu Rev Pharmacol Toxicol* 43:335-58
- 92 Williams SR, Stuart GJ (2003) Role of dendritic synapse location in the control of action potential output. *Trends Neurosci* 26(3):147–154
- 93 Wittenberg GM, Wang SS (2006) Malleability of spike-timing-dependent plasticity at the CA3-CA1 synapse. *J Neurosci* 26(24):6610-7
- 94 Wong RW, Setou M, Teng J, Takei Y, Hirokawa N (2002) Overexpression of motor protein KIF17 enhances spatial and working memory in transgenic mice. *Proc Natl Acad Sci U S A* 99:14500-5
- 95 Xia Z, Storm DR (2005) The role of calmodulin as a signal integrator for synaptic plasticity. *Nat Rev Neurosci* 6:267-76

- 96 Yang SN, Tang YG, Zucker RS (1999) Selective induction of LTP and LTD by postsynaptic  $[Ca^{2+}]_i$  elevation. *J Neurophysiol* 81(2):781-7
- 97 Yasuda H, Barth AL, Stellwagen D, Malenka RC (2003) A developmental switch in the signaling cascades for LTP induction. *Nat Neurosci* 6(1):15-6